



HAL
open science

Suppression of underlying neuronal fluctuations mediates EEG slowing during general anaesthesia

Axel Hutt, Jeremie Lefebvre, Darren Hight, Jamie Sleigh

► **To cite this version:**

Axel Hutt, Jeremie Lefebvre, Darren Hight, Jamie Sleigh. Suppression of underlying neuronal fluctuations mediates EEG slowing during general anaesthesia. *NeuroImage*, 2018. hal-02939283

HAL Id: hal-02939283

<https://inria.hal.science/hal-02939283>

Submitted on 18 Sep 2020

HAL is a multi-disciplinary open access archive for the deposit and dissemination of scientific research documents, whether they are published or not. The documents may come from teaching and research institutions in France or abroad, or from public or private research centers.

L'archive ouverte pluridisciplinaire **HAL**, est destinée au dépôt et à la diffusion de documents scientifiques de niveau recherche, publiés ou non, émanant des établissements d'enseignement et de recherche français ou étrangers, des laboratoires publics ou privés.

1 **Suppression of underlying neuronal fluctuations mediates EEG**
2 **slowing during general anaesthesia**

3 Axel Hutt¹, Jérémie Lefebvre², Darren Hight^{3 4}, Jamie Sleight^{3,*}

4 ¹*Department FE 12 – Data Assimilation , Deutscher Wetterdienst, 63067 Offenbach am Main, Germany*
5 *Department of Mathematics and Statistics, University of Reading, Reading RG6 6AX,UK*

6
7 ²*Krembil Research Institute, University Health Network, Toronto, Ontario M5T 2S8, Canada*
8 *Department of Mathematics, University of Toronto, Toronto, Ontario M5T 2S8, Canada*
9 *Institute of Biomaterials and Biomedical Engineering, University of Toronto, Toronto, Ontario M5T*
10 *2S8, Canada*

11
12 ³*Department of Anaesthesiology, Waikato Clinical Campus, University of Auckland, Hamilton 3240,*
13 *New Zealand*

14
15 ⁴*Department of Anaesthesiology and Pain Therapy, University Hospital Bern, Inselspital, Bern,*
16 *Switzerland*

17
18 Short title: Random fluctuations slow anaesthesia EEG

19
20 Keywords : anaesthesia, noise, functional fragmentation, alpha-activity

21
22 Corresponding author:

23 Axel Hutt

24 Deutscher Wetterdienst

25 Department FE12- Data Assimilation

26 Frankfurter Strasse 135

27 63067 Offenbach am Main , Germany

28 Tel.: +49 69 80622750 , Email: digitalesbad@gmail.com

29

30 **Abstract**

31 The physiological mechanisms by which anaesthetic drugs modulate oscillatory brain activity
32 remain poorly understood. Combining human data, mathematical and computational analysis of
33 both spiking and mean-field models, we investigated the spectral dynamics of encephalographic
34 (EEG) beta-alpha oscillations, observed in human patients undergoing general anaesthesia. The
35 effect of anaesthetics can be modelled as a reduction of neural fluctuation intensity, and/or an
36 increase in inhibitory synaptic gain in the thalamo-cortical circuit. Unlike previous work, which
37 suggested the primary importance of gamma-amino-butyric-acid(GABA) augmentation in causing a
38 shift to low EEG frequencies, our analysis demonstrates that a non-linear transition, triggered by a
39 simple decrease in neural fluctuation intensity, is sufficient to explain the clinically-observed
40 appearance – and subsequent slowing – of the beta-alpha narrowband EEG peak. In our model,
41 increased synaptic inhibition alone, did not correlate with the clinically-observed encephalographic
42 spectral changes, but did cause the anaesthetic-induced decrease in neuronal firing rate. Taken
43 together, our results show that such a non-linear transition results in functional fragmentation of
44 cortical and thalamic populations; highly correlated intra-population dynamics triggered by
45 anaesthesia decouple and isolate neural populations. Our results are able to parsimoniously unify
46 and replicate the observed anaesthetic effects on both the EEG spectra and inter-regional
47 connectivity, and further highlight the importance of neural activity fluctuations in the genesis of
48 altered brain states.

49

50

51 **Introduction**

52 General anaesthesia is a widely used medical procedure in today's clinical practice. One of the main
53 obstacles in the optimization of general anaesthesia is the limited understanding of the
54 physiological mechanisms behind anaesthetic actions and their consequences on neural
55 information processing.

56 One of the prominent effects of most commonly used anaesthetic drugs is the induction of
57 characteristic changes in the spectral properties of electrophysiological activity across cortical
58 brain areas and spanning multiple frequency bands (1, 2, 3, 4). These spectral changes have been
59 used as the basis for many monitoring indices of electroencephalographic data (EEG) measured
60 empirically during anaesthesia (5), and as such constitute one of the most reliable biomarkers of
61 the brain's arousal state. One of the most salient spectral changes observed in clinical practice is the
62 generation of prominent oscillatory activity in the β -frequency band (12 Hz -20 Hz) and its
63 subsequent gradual decrease to the α -frequency band (8 Hz -12 Hz) with increasing anaesthetic
64 concentration (6).

65 This slowing down in oscillatory neural activity has also been shown to correlate strongly with
66 patients' behavioural state. Indeed, in parallel to the encephalographic deceleration from β - to α -
67 activity, subjects' behavioural state changes from a sedated state to one of loss of responsiveness –
68 which we may equate with loss of connected consciousness (LOC).

69 Previous theoretical and computational studies have developed neural network models (7, 8) as
70 well as neural mass models (9, 10) to reproduce both β - and α -activity as observed across the
71 different states of anaesthesia. While insightful, these studies use network models with the limiting
72 assumptions of single anaesthetics acting on specific synaptic receptors or isolated ion channels,
73 and do so symmetrically across all neurons in a given circuit. From a practical perspective

74 however, mixtures of different classes of anaesthetic agents – as opposed to only one agent – are
75 almost always used in clinical settings to induce general anaesthesia. These combinations of
76 anaesthetic drugs are known to interact with each other (11), and are thus likely to impact neurons
77 and neuronal populations in heterogeneous ways. In the absence of known physiological
78 mechanisms and detailed information about anaesthetics interactions, it remains highly challenging
79 to model, yet properly characterize, general anaesthesia from the single neuron perspective.

80 In contrast to previous studies where the characteristic slowing of EEG rhythms is caused by
81 changes in single neuron properties (often modelled as slowing of the inhibitory post-synaptic
82 potential decay time), we here propose an alternative mechanism: that the characteristic EEG
83 slowing is driven by *system-level interactions*. Using human data, and based on our mathematical
84 and computational analysis of both spiking and mean-field models, we have found that the
85 oscillatory transitions, commonly observed across sedation stages, appear to be a characteristic
86 signature of non-linear systems undergoing a phase transition: brain dynamics switches between
87 different dynamical states, accompanied by an amplification of coherent activity. To provide deeper
88 insight into the neural mechanism of anaesthetics from a circuit point of view, our work shows that
89 anaesthetic action results in an effective decrease in broadband neural activity i.e. the neural
90 activity exchanged between neural structures involved becomes more regular and coherent. This
91 hypothesis is in full agreement with converging lines of evidence showing that neural activity in
92 awake human subjects and animals is highly irregular compared to activity under anaesthesia;
93 which has very limited spatio-temporal information content (3, 12-15). A previous study (16)
94 demonstrated nicely that spatial frontal coherence in the α -frequency increases markedly at the
95 point when subjects lose consciousness.

96 We considered a thalamo-cortical circuit of spiking neurons subjected to additive external random
97 fluctuations. When the fluctuation variance increases (as occurs during emergence from

98 anaesthesia), mathematical and computational analysis reveals an oscillatory transition that is a
99 characteristic signature of non-linear systems. With decreasing variance of fluctuations (as occurs
100 with increasing depth of anaesthesia), the opposite occurs and the system exhibits an amplification
101 of coherent dynamics. The corresponding connectivity analysis reveals *enhanced intra-area*
102 *synchrony* but a simultaneous *breakdown of inter-area synchrony*. Taken together, our results
103 support previously proposed hypotheses (17) in which anaesthesia represents a *systemic isolation*
104 of neural populations via a switch from globally-driven to locally-driven activity. Taken together,
105 our results show that circuit-scale interactions – as opposed to single neuron properties – are
106 mandatory to replicate the slowing down of EEG activity observed in human clinical data.

107

108 **Materials and Methods**

109 **Experimental data**

110 Experimental EEG data have been obtained from two patients recorded for a previous
111 observational study (6). This had institutional ethics approval (from the New Zealand Health and
112 Disability Ethics Committee, Ref. 12/CEN/56, 2013) and written informed consent. These patients
113 were both female (aged 29 and 77), and had anaesthesia initiated by a single dose of propofol, and
114 subsequently maintained by the volatile anaesthetic sevoflurane during their surgery.

115 The data under study was recorded from a frontal position (Fp_{1/2} – Fp_z in the 10-20 system) using a
116 Bispectral Index depth of anaesthesia monitor (BIS ®, Covidien, Boulder, CO, USA) at a sampling
117 frequency of 128 Hz, which was then down-sampled to 100 Hz. High and low pass non-phase
118 shifting Butterworth filters were applied to the data (at 0.25 and 48.5 Hz cutoffs respectively, both
119 set at 3dB). We have analyzed the temporal evolution of the frequency content of experimental data

120 by computing its spectrogram with window width $T=10s$ yielding a frequency resolution of 0.1Hz
121 and window overlap of 0.1s.

122

123 **Anaesthetic action of the ascending arousal system**

124 Anaesthetics affect neural communication by modifying synaptic receptor and ion channel
125 properties. It has been shown previously (18) that increasing anaesthetic concentrations diminish
126 thalamic input to the cortex and reduces thalamic and cortical firing activity caused by reduced
127 activation in the ascending arousal system (AAS, 19). Since the input to the cortex and the thalamus
128 is rather complex and not known in all detail, we consider external input as random fluctuations
129 with a certain mean and variance. Our underlying model considers neural population activity and
130 the random fluctuations represent an uncorrelated synaptic bombardment with high input
131 population firing.

132 To estimate the anaesthetic action on the amplitude of those random fluctuations, we consider a
133 simple neural network describing anaesthetic action in the AAS (19, 20). Several clinically relevant
134 anaesthetics affect GABAergic synaptic and extra-synaptic receptors in the AAS inducing phasic and
135 tonic inhibition, respectively (2,21). For instance, GABAergic synaptic receptors are present in the
136 AAS-structures brainstem, hypothalamus and the basal forebrain (2,21) and anaesthetics prolong
137 their phasic response. Extra-synaptic receptors occur primarily in sub-cortical structures such the
138 brainstem, hypothalamus and thalamus (10,22) and anaesthetics enhance the tonic inhibitory
139 current.

140 The AAS exhibits a rather complex network of interacting structures that inhibit each other
141 according to diverse direct and indirect actions. Previous experimental and theoretical studies of
142 phasic and tonic inhibition (23) have shown that increasing the synaptic time constant and

143 decreasing the pre-synaptic firing rate decreases the synapses phasic response variance. This
 144 indicates decreased response mean and variance with increased anaesthetic action by prolonged
 145 post-synaptic phasic response and enhanced pre-synaptic firing reduction by tonic inhibition. To
 146 show this anaesthetic impact, we consider anaesthetic actions on both phasic and tonic inhibition in
 147 our simplified model of the AAS. To illustrate the phasic and tonic inhibition separately and clarify
 148 their action, we distribute phasic and tonic receptors over different populations. A chain of three
 149 neural populations of spiking neurons (Fig.1(a)) reflect the functional structure of AAS. The first
 150 two populations exhibit tonic and phasic inhibition and the last population sums up the output
 151 providing the random fluctuations (Fig.1(a)). These fluctuations may represent the input to
 152 thalamic structures or to the cortex.

153 The first population (neurons t in Fig.1(a)) includes uncoupled Leaky Integrate-and-Fire neurons
 154 (LIF) of number $N=80$ with tonic inhibition (23,24). The neurons are driven by a constant input
 155 current. Such neurons may be located in brainstem structures, such as the *locus coeruleus* or
 156 *parabrachial nucleus* that project to a large part of the cortex and thalamus. Their membrane
 157 potential V_n obeys

$$C \frac{dV_n}{dt} = g_l(E_l - V_n) + g_t(E_t - V_n) + I, \quad n = 1, \dots, N$$

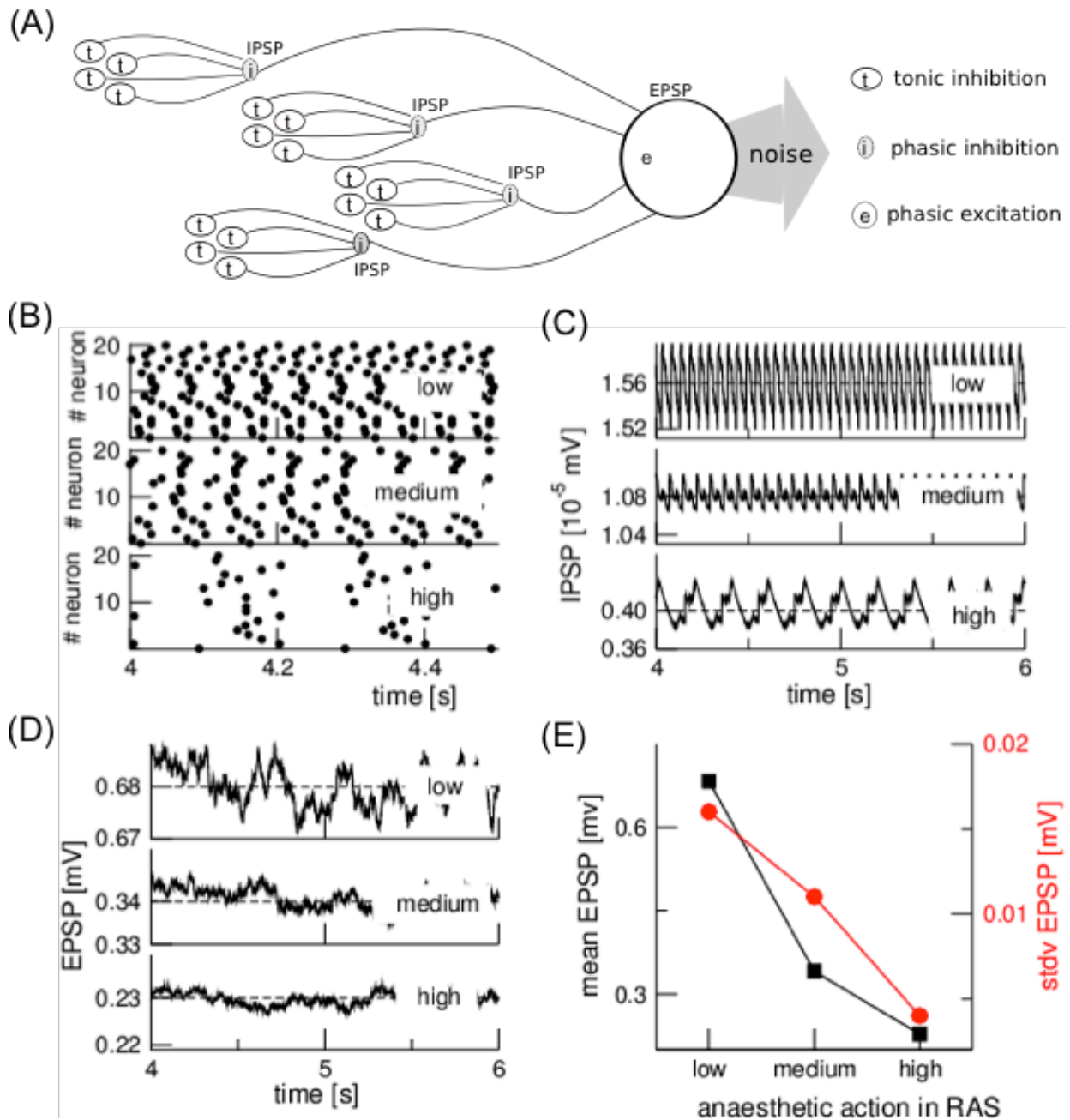
158 for $V_n < \theta_n$. The thresholds θ_n are random and uniformly distributed about the mean threshold
 159 $\theta = -58mV$ in the range $[-59.5mV; -56.5mV]$. The reset potential is $V_{reset} = -68mV$ and an $8ms$
 160 refractory time is chosen. The other parameters are the capacity $C = 33nF$, the constant leak
 161 conductance $g_l = 22nS$, the leak reversal potential $E_l = -76mV$ and the synaptic reversal potential
 162 $E_t = -76mV$. The external current is $I = 8nA$. The tonic conductance takes values $g_t = 0nS$
 163 , $g_t = 200nS$ and $g_t = 400nS$ that represent low, medium and high tonic anaesthetic action,
 164 respectively. In the numerical simulations, initial conditions are random and distributed uniformly

165 in the interval $[V_{reset} - 15mV; V_{reset} + 15mV]$. Figure 1(b) shows raster plots for the three
166 anaesthetic levels. The larger the inhibitory tonic current, the lower is the firing rate in accordance
167 to previous studies (23,24).

168 These neurons emit spikes targeting inhibitory GABAergic synapses (neurons i in Fig.1(a)) of
169 number N with an exponential response function of time scale τ . Such synapses may be located in
170 the hypothalamus, e.g. in the *ventrolateral preoptic nucleus*, receiving projections from the
171 brainstem. Hence the inhibitory response potential $IPSP_m$ at post-synaptic neuron m obeys

$$\tau \frac{dIPSP_m}{dt} = -IPSP_m + s_m, m = 1, \dots, N$$

172 where $s_m = 1mV$ when pre-synaptic spikes arrive and $s_m = 0$ otherwise. Anaesthetics prolong the
173 synaptic time scale and we choose $\tau = 200ms$, $\tau = 400ms$, and $\tau = 600ms$ for low, medium and
174 high anaesthetic impact, respectively. Figure 1(c) presents the sum of these synaptic responses
175 $IPSP(t) = \sum_{m=1}^N IPSP_m(t)$ and reveals reduced magnitude and bias of post-synaptic currents with
176 increased anaesthetic action.



177

178 Figure 1: Effect of the ascending arousal system on cortical and thalamic activity. (A) Topology of
 179 the simulated network. (B) Spike trains of the output of tonic inhibition neurons targeting phasic
 180 inhibition neurons for different anaesthetic action levels (C) Inhibitory post-synaptic potentials
 181 (IPSP) evoked by spike trains in (B). (D) Excitatory post-synaptic potentials (EPSP) that describes

182 the noise applied to the cortico-thalamic network. (E) Both mean and standard deviation of EPSP
183 decrease with the anaesthetic action level.

184 The summed-up inhibitory current triggers the spike discharge in the post-synaptic neuron what is
185 modeled as a Poisson neuron with firing rate $\lambda(t) = f[IPSP(t)]$ with the transfer function
186 $[U] = \frac{100Hz}{1+e^{-(U-\vartheta)}}$, $\vartheta = 8\mu V$. We consider $M=40$ of such Poisson neurons whose spike discharges
187 target excitatory synapses (neuron e in Fig.1(a)) with exponential response function and constant
188 time scale of $20ms$. Such synapses may be located in the thalamus or the cortex. The sum of these
189 excitatory responses $EPSP$ represents the random fluctuations. Figure 1(d) demonstrates that
190 stronger anaesthetic action decreases the magnitude of EPSPs and its bias. Since this EPSP
191 describes the input of the AAS to thalamus and cortex, we summarize that increasing anaesthetic
192 action reduces the variance of input fluctuations and its bias. These results are summarized in
193 Fig.1(e). This finding is consistent with recent experimental evidence in rats showing that
194 somatosensory and primary motor neurons in the anaesthetic-induced isoelectric state are fully
195 responsive to external stimuli (55). This finding is affirmed qualitatively for humans in the same
196 study. Since anaesthetic isoelectric states emerge under deep anaesthesia, this result demonstrates
197 that neurons are not strongly inhibited in deep anaesthesia as it would be the case if synaptic
198 inhibition alone would be present. We argue that anaesthetic action rather diminishes the input
199 from AAS to these neurons and, in this way, retain their responsiveness.

200 In the following we modify the fluctuation variance and keep the bias constant for the frontal
201 cortico-thalamic model. This approximation is reasonable since additional studies (not shown)
202 revealed that the major results in the present work are invariant for small anaesthetic-induced bias
203 adaptation. In the occipital cortico-thalamic model, we modify both the fluctuation variance and the
204 bias. We find that the additional bias reduction is mandatory to reproduce qualitatively the occipital

205 power reduction. For simplicity, mentioning the fluctuation variance in the following discussion of
 206 the occipital model always implies a synchronous bias reduction.

207

208 **Anaesthetic action in the frontal cortico-thalamic network**

209 The relation proposed above between anaesthetic action and input variance does not specify in
 210 detail the relation between fluctuation variance and anaesthetic action of different anaesthetic
 211 agents in the cortex and sub-cortical structures. We hypothesize that this relationship is an effective
 212 approximation of anaesthetic action and it is valid for various combinations of anaesthetic agents.
 213 Our analysis suggests that this represents one of the major mechanisms of such pharmacological
 214 agents on thalamocortical populations.

215 We assume that neuron ensembles in the cortex and thalamus are subjected to endogenous,
 216 background sources of inputs $A_k^j(t) = \sqrt{2D} \xi_k^j(t)$ with $k=e, I, th, rtn$ for the cortical excitatory (e),
 217 cortical inhibitory (i), thalamic *lateral geniculate nucleus* (th) and thalamic reticular (rtn)
 218 population (cf. Fig.2(A)). Here, $\xi_k^j(t)$ are independent random Gaussian processes with identical
 219 variance. Anaesthetic action in the cortex and thalamus is modeled by changing the level of noise or
 220 fluctuation variance D in the system with increasing anaesthetics concentration in accordance to
 221 the AAS-model. In numerical experiments, the variance either obeys the piece-wise exponential
 222 laws

$$223 \quad D(t) = D_1 e^{-t/\tau_n} + D_0, 0 \leq t_1,$$

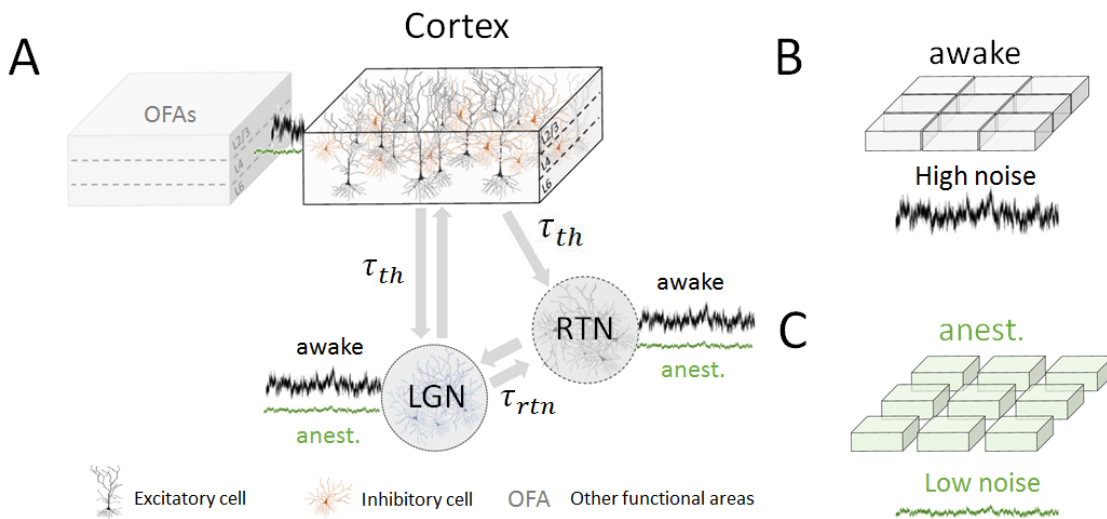
$$224 \quad D(t) = D_2, t_1 < t \leq t_2, \tag{1}$$

$$225 \quad D(t) = D_4 e^{t/\tau_n} + D_3, t_2 < t \leq t_3,$$

226 with $\tau_n, D_0, D_1, D_4 > 0, D_2 = D_1 e^{-t_1/\tau_n} + D_0, D_3 = D_2 - D_4 e^{t_2/\tau_n}$ or the linear model

227
$$D(t) = -mt + D_5, 0 \leq t \leq t_1 \tag{2}$$

228 with $D_0 > 0, m > 0$. For Eqs. (1), we choose parameters such that $D(0) = 1.01, D_2 = 0.01, D(t_3) =$
 229 0.04 with $t_1 = t_3/2, t_2 = 0.6t_3, t_3 = 32.768s, \tau_n = (32786/0.16)s$. In the linear model in Eq. (2)
 230 $D_5 = 0.345, m=0.005$ with $t_1 = 32.768s$. Here, the temporal duration in both simulations is
 231 $32.768s$.



232
 233 *Figure 2: Illustration of thalamo-cortical network subjected to additive random fluctuations. (A)*
 234 *network topology (B) decreasing fluctuation variance functionally decouples the network.*

235
 236 We assume that this effective reduction of fluctuation variance represents the major effect of
 237 anaesthetics on the cortico-thalamic circuit. In addition to the effect of fluctuations, it has been
 238 shown in numerous experimental studies that a large variety of anaesthetic drugs inhibits neural

239 activity by action on GABAergic synaptic receptors. To take into account this synaptic effect , we
 240 included a prolongation of the synaptic decay time scale of inhibitory GABAergic receptors while
 241 retaining the amplitude of the synaptic inhibitory impulse response. Mathematically the synaptic
 242 decay time scale of GABAergic synapses obey

$$243 \quad \tau_i(t) = \tau_i^0 p(t) .$$

244 When utilizing the exponential fluctuation variance model, the factor synaptic decay time scale
 245 factor obeys the linear law

$$246 \quad p(t) = 1 + 2t/t_1 , 0 \leq t_1 ,$$

$$247 \quad p(t) = 3 , t_1 < t \leq t_2 ,$$

$$248 \quad p(t) = 3 - 2(t - t_2)/(t_3 - t_2) , t_2 < t \leq t_3$$

249 with the same times t_1 , t_2 and t_3 as in (1). The corresponding the linear model is $p(t) = 1 +$
 250 $2t/t_1$, $0 \leq t_1$. This anaesthetic model is motivated by a previous study based on experimental data
 251 (51).

252 **Anaesthetic action in the occipital cortico-thalamic network**

253 The occipital anaesthetic action model is very similar to the frontal model. Since not much is known
 254 about the projection targets of the AAS to the occipital cortex, we consider a diffusive projection to
 255 the cortex via the basal forebrain (19,56) but neglect AAS stimulation of thalamic structures. To
 256 illustrate the spectral power dynamics with decreasing AAS activity, we assume the fluctuation
 257 variance D to decrease in time according to

$$D(t) = D_1 e^{-t/\tau_n} + D_0 , 0 \leq t \leq t_1$$

258 with $t_1 = 32.768$ s , $D(0) = 0.06$, $\tau_n = (32786/0.16)$ s and $D_0 = 0.0006$. The excitatory
 259 endogenous, fluctuating background input is $A_e^j(t) = \sqrt{2D} \xi_k^j(t)$, whereas other time-dependent
 260 input $A_i^j(t) = A_{th}^j(t) = A_{rtn}^j(t) = 0$. This is different to the frontal model, where all cortical and
 261 thalamic structures are driven by the AAS. Moreover, the mean excitatory input from AAS obeys the
 262 Hill equation

$$263 \quad I_e(t) = -0.5 - 3/(1 + (0.7t_1/t)^4), 0 \leq t \leq t_1 .$$

264 that is a decreasing sigmoidal function with turning point at $t = 0.7t_1$. The mean input to the other
 265 structures I_i, I_{th}, I_{rtn} remain constant. To consider anaesthetic effects on synaptic inhibition, the
 266 synaptic time scale factor increases over time according to

$$p(t) = 1 + 2/(1 + (1.5t_1/t)^4), 0 \leq t \leq t_1$$

267

268 **Spiking frontal model**

269 To understand the underlying neural mechanism of changes in EEG spectral features, we
 270 investigated a thalamo-cortical hybrid network model of Amari-type (25). The network is built of
 271 recurrently connected neural ensembles of excitatory pyramidal neurons (e) and inhibitory
 272 interneurons (i) interacting with thalamic relay (th) neurons in the Lateral Geniculate Nucleus
 273 (LGN) and thalamic reticular neurons (rtn), cf. Fig.2 (A) .

274 Spiking activity of those neural ensembles follow the non-homogeneous Poisson processes

$$275 \quad X_e^j(t) \rightarrow \text{Poisson}(f[u_e^j(t)]) , X_i^j(t) \rightarrow \text{Poisson}(f[u_i^j(t)])$$

$$276 \quad X_{th}^j(t) \rightarrow \text{Poisson}(f[u_{th}^j(t)]) , X_{rtn}^j(t) \rightarrow \text{Poisson}(f[u_{rtn}^j(t)])$$

277 where $X_{e,i,th,rtn}^j(t) = \sum_{\{t_l\}} \delta_{e,i,th,rtn}^j(t - t_l)$ is the spike train of the j^{th} ensemble patch in the
 278 respective population. The ensemble response function $f[u] = (1 + \exp\{-\beta(u - h)\})^{-1}$ represents
 279 a saturating firing rate function with gain $\beta = 150$ and threshold $h = 0.1$. The average potentials of
 280 ensemble j of excitatory and inhibitory neurons $u_e^j(t)$ and $u_i^j(t)$, respectively, and the thalamic
 281 potentials $u_{th}^j(t)$ and $u_{rtn}^j(t)$ obey

$$282 \quad \alpha_e^{-1} \frac{du_e^j(t)}{dt} = -u_e^j(t) + b v_e^j(t) + S_{e \rightarrow e}^j(t) + S_{i \rightarrow e}^j(t) + S_{th \rightarrow e}(t - \tau_{th}) + I_e + A_e^j(t) \quad (3)$$

$$\alpha_i^{-1} \frac{du_i^j(t)}{dt} = -u_i^j(t) + b v_i^j(t) + S_{e \rightarrow i}^j(t) + S_{i \rightarrow i}^j(t) + S_{th \rightarrow i}(t - \tau_{th}) + I_i + A_i^j(t)$$

$$\alpha_{th}^{-1} \frac{du_{th}^j(t)}{dt} = -u_{th}^j(t) + b v_{th}^j(t) + S_{e \rightarrow th}^j(t - \tau_{th}) + S_{rtn \rightarrow th}^j(t - \tau_{rtn}) + I_{th} + A_{th}^j(t)$$

$$\alpha_{rtn}^{-1} \frac{du_{rtn}^j(t)}{dt} = -u_{rtn}^j(t) + b v_{rtn}^j(t) + S_{e \rightarrow rtn}^j(t - \tau_{th}) + S_{th \rightarrow rtn}^j(t - \tau_{rtn}) + I_{rtn} + A_{rtn}^j(t)$$

$$283 \quad \alpha^{-1} \frac{dv_e^j(t)}{dt} = -v_e^j(t) + u_e^j(t) ; \alpha^{-1} \frac{dv_i^j(t)}{dt} = -v_i^j(t) + u_i^j(t)$$

$$284 \quad \alpha^{-1} \frac{dv_{th}^j(t)}{dt} = -v_{th}^j(t) + u_{th}^j(t) ; \alpha^{-1} \frac{dv_{rtn}^j(t)}{dt} = -v_{rtn}^j(t) + u_{rtn}^j(t)$$

285 where $v_n^j(t)$ refers to corresponding adaptation currents, b is the adaptation gain and $S_{n \rightarrow m}^j$ are
 286 synaptic inputs from population n to population m . The variables $u_n^j(t)$ represent the Local Field
 287 Potential that would be measured with an implanted electrode in population $n = e, i, th, rtn$. The
 288 terms I_n are constant bias currents and A_n^j are random external input currents. Cortico-thalamic
 289 interactions are delayed by a propagation delay τ_{th} , while we have also included an interaction
 290 delay τ_{rtn} between LGN and the reticular population. In addition, local, distance-dependent
 291 propagation delays are also included within the cortical populations. Using these, the resulting
 292 integrated synaptic inputs to the neurons are given by

$$S_{n \rightarrow m}^j(t) = N_n^{-1} \sum_{k=1}^{N_n} W_{n \rightarrow m}^{jk} \cdot E_{nm}^k(t - \tau^{jk}).$$

293 The individual propagation delays are given by $\tau^{jk} = \Delta^{jk}/c$, where c is a finite conduction velocity
 294 and Δ^{jk} is the spatial distance between ensemble patch of number j and k . Ensembles are
 295 distributed randomly and uniformly within a one dimensional spatial domain Ω of length $|\Omega|$.
 296 Average post-synaptic potentials $E_n^k(t)$ are computed as input spike trains convolved with
 297 exponential synapses with time constant τ_m

$$E_{nm}^k(t) = \int_0^t X_n^k(s) \frac{1}{\tau_m} e^{-(t-s)/\tau_m} ds.$$

298 As pointed out above, $\tau_i = \text{const}$ or $\tau_i = \tau_i(t)$ in two studies. Recurrent synaptic weights amongst
 299 ($W_{n \rightarrow n}^{jk}$) and between ($W_{n \rightarrow m}^{jk}$) excitatory and inhibitory populations exhibit sparse Gaussian profiles

$$W_{n \rightarrow m}^{jk}(\rho) = \frac{w_{n \rightarrow m}^o(\rho)}{\sqrt{2\pi\sigma_{n \rightarrow m}^2}} \exp\left[-\frac{(\Delta^{jk})^2}{2\sigma_{n \rightarrow m}^2}\right]$$

300 where $w_{n \rightarrow m}^o(\rho) = w_{n \rightarrow m}^o \neq 0$ with probability ρ . Model constants are given in Table 1. The
 301 numerical integration step is $\Delta t = 0.001s$ and all variables have been initialized in $t \in [-\tau; 0]$ to
 302 $u_n, v_m = 0$ with the maximum delay time τ .

303 **Table 1: Table of Model Parameters**

Symbol	Definition		Symbol	Definition	
Ω	Network spatial extent [mm]	10	ρ	Connection probability	0.2
N_e	Number of excitatory cells	800	$w_{e \rightarrow e}^o$	Synaptic connection strength	12
N_i	Number of inhibitory cells	200	$w_{e \rightarrow i}^o$	Synaptic connection strength	-25
N_{th}	Number of thalamic cells	200	$w_{i \rightarrow e}^o$	Synaptic connection strength	25
N_{rtn}	Number of reticular cells	200	$w_{i \rightarrow i}^o$	Synaptic connection strength	-12
β	Neural response function gain [1/mV]	150	$w_{e \rightarrow th}^o$	Synaptic connection strength	5

h	Firing rate threshold [Hz]	1	$w_{e \rightarrow rtn}^o$	Synaptic connection strength	5
τ_m	mean time constant [s]	1	$w_{th \rightarrow e}^o$	Synaptic connection strength	35
α_e	mean rate constant – excitatory cortical cells [Hz]	1.0	$w_{th \rightarrow i}^o$	Synaptic connection strength	-10
α_i	mean rate constant – inhibitory cortical cells [Hz]	1.5	$w_{th \rightarrow rtn}^o$	Synaptic connection strength	12
α_{th}	mean rate constant – thalamic neurons [Hz]	0.2	$w_{rtn \rightarrow th}^o$	Synaptic connection strength	12
α_{rtn}	mean rate constant – reticular cells [Hz]	0.2	$\sigma_{e \rightarrow e}^2$	Synaptic connection range [mm]	0.1
a	Neural adaptation rate constant [Hz]	0.005	$\sigma_{e \rightarrow i}^2$	Synaptic connection range [mm]	0.1
b	Neural adaptation gain [1/s]	0.1	$\sigma_{i \rightarrow e}^2$	Synaptic connection range [mm]	2.5
I_e	Constant current bias [mV/s]	0	$\sigma_{i \rightarrow i}^2$	Synaptic connection range [mm]	2.5
I_i	Constant current bias [mV/s]	0	$\sigma_{e \rightarrow th}^2$	Synaptic connection range [mm]	0.1
I_{th}	Constant current bias [mV/s]	0.1	$\sigma_{e \rightarrow rtn}^2$	Synaptic connection range [mm]	0.1
I_{rtn}	Constant current bias [mV/s]	-0.5	$\sigma_{th \rightarrow e}^2$	Synaptic connection range [mm]	2.5
τ_{th}	Thalamo-cortical delay [ms]	2	$\sigma_{th \rightarrow i}^2$	Synaptic connection range [mm]	2.5
τ_{rtn}	Reticular-thalamic delay [ms]	2	$\sigma_{th \rightarrow rtn}^2$	Synaptic connection range [mm]	2.5
c	Conduction velocity [m/s]	0.35	$\sigma_{rtn \rightarrow th}^2$	Synaptic connection range [mm]	2.5
			dt	Integration time step [ms]	1

304

305 **Spiking occipital model**

306 The network topology of the occipital model is identical to that of the frontal model. However, by
307 virtue of the differences in intra-area neural structures and their different functional role in the
308 brain, some parameters are different. The time scale of the intra-cortical excitatory and inhibitory
309 adaption currents are chosen differently to

$$310 \quad a_e^{-1} \frac{dv_e^j(t)}{dt} = -v_e^j(t) + u_e^j(t) ; a_i^{-1} \frac{dv_i^j(t)}{dt} = -v_i^j(t) + u_i^j(t)$$

311 with $a_e = 1.0$, $a_i = 0.1$. This specific parameter choice in the full parameter set fixes the oscillation
312 frequency at large fluctuation variance to about 10Hz.

313

314 **Effective mean-field model**

315 To understand the macroscopic dynamics of the spiking neural network, it is insightful to consider
 316 its spatially averaged dynamics. Statistical features and average population dynamics of the cortical
 317 populations were exposed by investigating the mean-field formulation of the more fined grained
 318 spiking model above, leaving aside the LGN and reticular neurons. Using a mean-field
 319 approximation (26,27), the mean dynamics of the excitatory and inhibitory cortical potentials U_e
 320 and U_i can be shown to obey

$$321 \quad \alpha_e^{-1} \frac{dU_e}{dt} = -U_e + bV_e + \bar{W}_{e \rightarrow e} F_e[U_e(t - \tau)] + \bar{W}_{i \rightarrow e} F_i[U_i(t - \tau)] + I_e \quad (4a)$$

$$322 \quad \alpha_i^{-1} \frac{dU_i}{dt} = -U_i + bV_i + \bar{W}_{e \rightarrow i} F_e[U_e(t - \tau)] + \bar{W}_{i \rightarrow i} F_i[U_i(t - \tau)] + I_i \quad (4b)$$

$$323 \quad a_e^{-1} \frac{dV_e}{dt} = -V_e + U_e \quad (4c)$$

$$324 \quad a_i^{-1} \frac{dV_i}{dt} = -V_i + U_i, \quad (4d)$$

325 where the fluctuation-corrected neural response function reads

$$326 \quad F_k[U] = \frac{1}{2} \left[1 + \operatorname{erf} \left(\frac{U-h}{\sigma_k \sqrt{2}} \right) \right],$$

$$327 \quad \sigma_k = -\sqrt{2}D \left(\frac{A^2}{2\lambda_+} + \frac{2AB}{\lambda_+ + \lambda_-} + \frac{B}{2\lambda_-} \right)$$

$$328 \quad \lambda_{\pm} = (-a_k - \alpha_k \pm \sqrt{(a_k - \alpha_k)^2 + 4ba_k\alpha_k})/2, \quad A = \sqrt{2\pi} \frac{a+\lambda_+}{\lambda_+ - \lambda_-}, \quad B = -\sqrt{2\pi} \frac{a+\lambda_-}{\lambda_+ - \lambda_-}.$$

329 Here, σ_k is the standard deviation of colored random fluctuations about the mean-field neural
 330 activity and each neuron behaves like a McCulloch-Pitts neuron with $\beta \rightarrow \infty$. Since $\sigma_k \sim D$,
 331 decreasing the fluctuation variance renders the response function F_k steeper. Previous studies

332 have shown that this may diminish the frequency of synchronous oscillation (26). The coefficients
 333 $\bar{W}_{n \rightarrow m}$ stand for the mean synaptic connectivity weights, computed by averaging all entries within
 334 the associated random matrices.

335 To understand the solution dynamics of the mean-field model, we have calculated numerically the
 336 stationary state of the mean-field model $(\bar{U}_e, \bar{U}_i, \bar{V}_e, \bar{V}_i)$ and studied numerically the temporal
 337 dynamics of deviations $(u_e = U_e - \bar{U}_e, u_i = U_i - \bar{U}_i, v_e = V_e - \bar{V}_e, v_i = V_i - \bar{V}_i)$ from these states.
 338 Parameters used are $\bar{W}_{e \rightarrow e} = 2.21, \bar{W}_{e \rightarrow i} = 4.58, \bar{W}_{i \rightarrow e} = -3.46, \bar{W}_{i \rightarrow i} = -1.69, b = 0.1, a_e = a_i = 5.0$
 339 $, \alpha_e = 50.0, \alpha_i = 100.0, I_e = 0.1, I_i = 0, h = 0.1$.

340

341 **Spectral Analysis**

342 In the neural model, neuro-electric activity corresponds to a spatial summation of localized electric
 343 potentials emanating from superficial cortical neurons. We modeled the electroencephalographic
 344 $EEG(t)$ signal as the weighted spatial average

$$345 \quad EEG(t) = N_e^{-1} \sum_{k=1}^{N_e} \phi_e^k u_e^k(t) + N_i^{-1} \sum_{k=1}^{N_i} \phi_i^k u_i^k(t) \quad , \quad (5)$$

346 $\phi_{e,i}^k = [0,1]$ denote random, positive coefficients accounting for dispersion effects and other source
 347 of observational noise. Spectral analysis in the time-frequency domain was performed applying
 348 Morlet wavelet analysis with equidistant frequencies.

349

350 **Spike rate and spike coherence calculation**

351 The instantaneous firing rate is the estimated number of spikes of each neuron occurring in a time
 352 window of $5ms$. In our evaluation the spike rate depends on the linearly decreasing fluctuation

353 variance and we applied a sliding window of width $\Delta D = 0.01$. To evaluate statistically the change
 354 of spike rate, we applied a non-parametric Kruskal-Wallis test with respect to the firing rate at
 355 maximum fluctuation variance.

356 Mean spike coherence in the cortex was computed based on standard calculations (28), consisting
 357 of two randomly selected neurons i, j within the cortical population, and binning their respective
 358 responses over a given time window ΔT . Thus, for neuron j , $X_j^{bin}(k\Delta T) = 1$ if a spike occurred
 359 during the interval $[k\Delta T, (k + 1)\Delta T]$, and zero otherwise, where $k = T/\Delta T$. Intra-area coherence
 360 $\theta(\Delta T)$ was then computed using

$$\theta(\Delta T) = \frac{\sum_T X_i^{bin} Y_j^{bin}}{\sum_T X_i^{bin 2} \sum_T Y_j^{bin 2}}$$

361 for two spike trains X, Y in the same area. The spike activity under study is assumed to evolve on a
 362 large time scale compared to the rapid spike dynamics. Consequently it is reasonable to average
 363 θ over a time window of duration T . In order to evaluate the evolution of the spike coherence with
 364 changing fluctuation variance relative to the maximum fluctuation variance, we consider the
 365 relative spike coherence θ/θ_0 where θ_0 is the spike coherence with maximum variance D . In the
 366 simulations, we choose 100 randomly chosen pairs of neurons in the cortical E-population with a
 367 small time window $\Delta T = 5\text{ms}$ and $T = 1\text{s}$ ($\Delta D = 0,00005$ and a range of fluctuation variances of
 368 $D = 0.01$ in Figs. S3 and S4). Smaller time intervals ΔT retain the given results qualitatively. The
 369 significance test is non-parametric of Kruskal-Wallis type and verifies the significance of the spike
 370 coherence at various fluctuation variances compared to the maximum fluctuation variance.

371 In addition to the intra-area spike coherence, we compute the cross spike coherence between two
 372 different areas where X, Y are spike trains from the areas. The corresponding parameters are
 373 identical to the case of intra-area spike coherence, but for 300 randomly chosen pairs of neurons
 374 from the different populations. All given spike coherence estimates are ratios to the spike

375 coherence at the largest fluctuation variance. The Kruskal-Wallis test verifies the significance of
376 cross coherences compared to cross coherences at the maximum fluctuation variance.

377 **Spike Field Coherence**

378 Spike Field Coherence (SFC) reflects the synchronization between spikes and corresponding
379 electric potentials (29). To estimate the SFC in the cortex at large and small fluctuations, we
380 compute it in both cases in a time window of 5s in the δ –(0.5Hz-4Hz), θ –(4Hz-8Hz), α –(8Hz-
381 12Hz) and β –(12Hz-20Hz) frequency band. This standard measure estimates the coherence
382 between spikes and their corresponding electric potentials at the same cell averaged over all cells.

383 In addition, we estimate the spike-field coherence between cortical EEG and spiking activity in the
384 LGN cells and the reticular cell. The corresponding cross-SFC represents the coherence between
385 thalamic spikes and cortical EEG at the same time instant averaged over all cells.

386

387 **Global phase synchronization**

388 Phase synchronization (PS) is a measure of the phase consistency between two time series. In our
389 case, the PS between two populations in the network model is obtained by comparing the phase
390 between their respective mean potential activities. Typically PS is non-stationary and subject to
391 random fluctuations. The instantaneous phase-locking value (PLV) represents a statistical estimate
392 of the degree of constant phase relation between several time series in a certain time interval and a
393 certain frequency band (30). In fact, the PLV is the instantaneous circular variance of the phase
394 difference of two time series. We take up this definition and compute a global PS index (GPS) by
395 (31)

$$396 \quad GPS = \left| \frac{1}{N} \sum_{k=1}^N e^{-i\Delta\varphi_k} \right|^2 \quad ,$$

397 $\Delta\varphi_k$ is the phase difference in the time series pair k at a certain time instance and N is the number
398 of phase pairs considered. In practice, typically one averages over a set of pairs and time instances
399 in a certain time window. The Results section shows values of GPS gained by a Morlet wavelet
400 transform in the frequency range [1Hz;20Hz] based on E-population Local Field Potentials down-
401 sampled to a sampling frequency of 50 Hz. We have chosen randomly 20 pairs of neurons out of
402 100 fixed randomly chosen neurons and averaged over 10 independent trials.

403 Instantaneous phases are defined mathematically in the case of non-vanishing instantaneous
404 amplitudes only and may be spurious for very low amplitudes. We define numerical phase values
405 φ_l from single time series l in the E-population to be valid only if its amplitude exceeds a threshold.
406 This threshold is set to be half of the amplitude of the space-averaged activity at the same time
407 instance and frequency band. This conservative criterion reduces the number of spurious phase
408 synchronization indices dramatically and hence ensures the validity of the GPS.

409

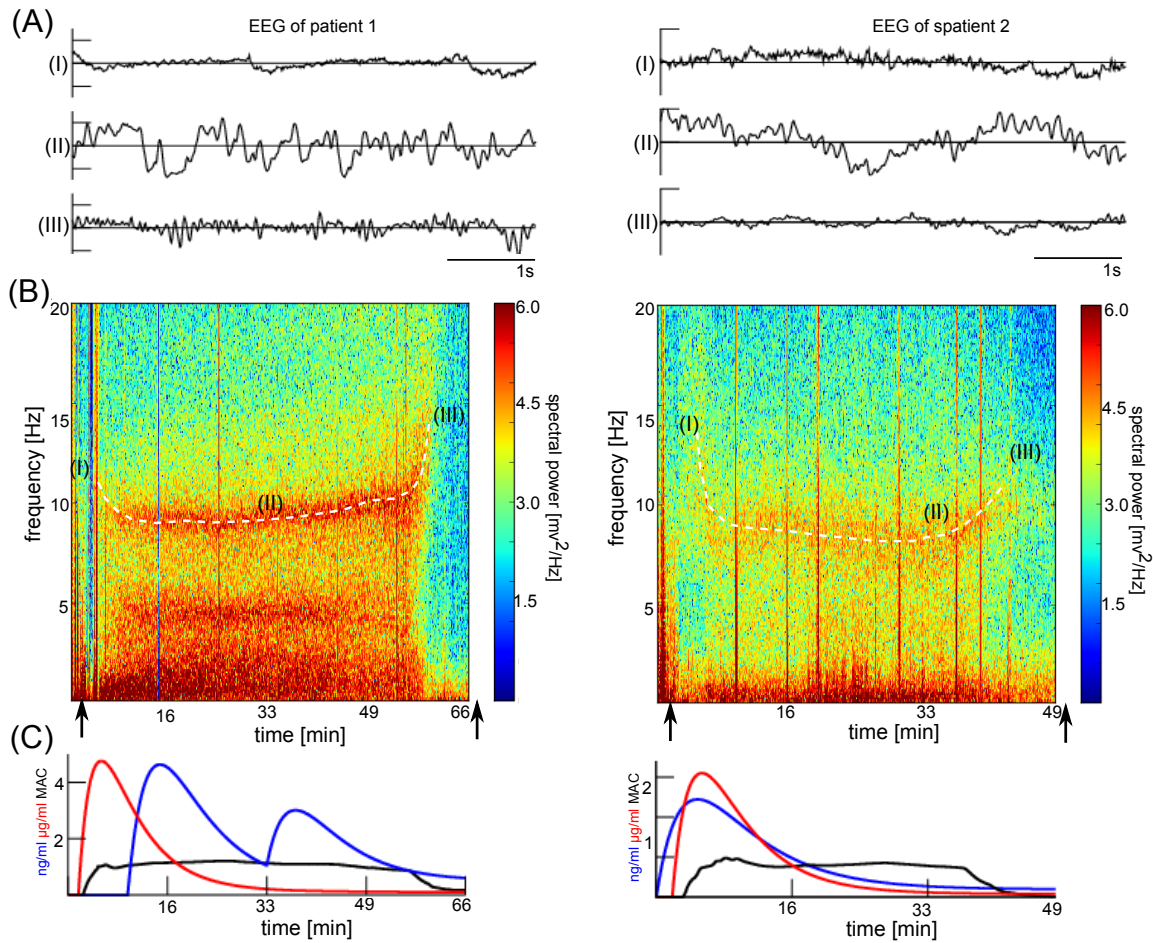
410 **Results**

411 *Experimental Data*

412 Figure 3A illustrates the characteristic temporal evolution of EEG obtained experimentally in two
413 patients: (I) at the beginning of the surgery during light anaesthesia, (II) during deep anaesthesia
414 and (III) during the awake phase after surgery. The spectral content of the EEG during the full
415 course of surgery is shown in Fig. 3B. We note that before the start of anaesthetic administration,
416 the EEG exhibits artefactual activity in the delta-frequency range, caused by movement and muscle
417 activity. After the onset of propofol (cf. Fig.1C, red curve), oscillations in the β -band emerge and
418 gradually slow down towards the alpha-band, cf. white dashed line in Fig. 1B. In both of these
419 patients, the analgesic fentanyl was also given, and the subsequent maintenance of general

420 anaesthesia was achieved by the volatile agent sevoflurane. After several minutes of anaesthetic
421 administration, the power peak frequency saturates in the α -frequency band while increasing its
422 spectral power. Moreover, the initial high fentanyl concentration enhances activity in the δ -
423 frequency band. At the end of surgery, the anaesthetic concentration decreases and the patient
424 emerges back to full consciousness (outside the time interval shown in Fig. 1). This emergence
425 phase is nicely reflected by an increase in the frequency of the peak power; from the α -range back
426 to the β -frequency range, and then followed by a suppression of oscillatory power in that
427 frequency band. There is also a decrease of power in the δ -frequency band. In these cases, the
428 emergence phase qualitatively resembles a backward loss of consciousness phase transition. This
429 oscillatory pattern is called the *smile* effect due to the spectrogram trajectory of the peak frequency.
430 Notice that in both subjects, the oscillatory transition observed is similar despite the big differences
431 in the anaesthetic concentrations.

432



433

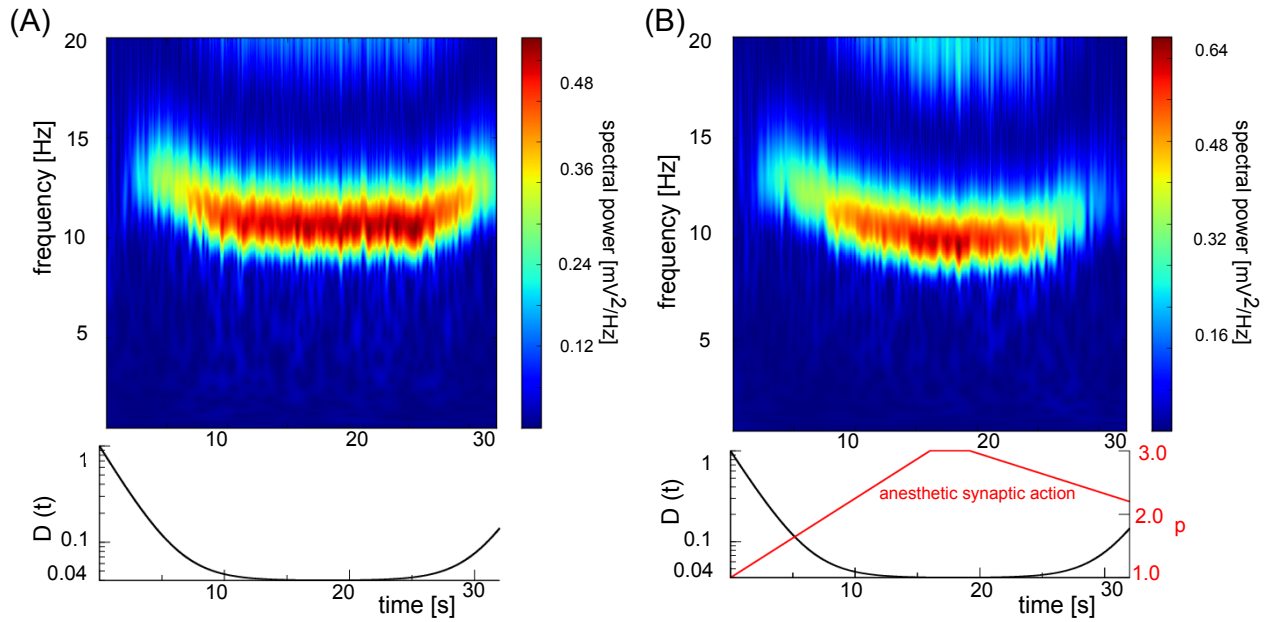
434 Figure 3: Characteristic *smile effect* observed in experimental frontal EEG spectral data. (A) Time
 435 series of experimental frontal EEG from two patients obtained at different moments in time during
 436 surgery, see (B) for encoded time points. (B) Spectral power distribution of experimental EEG data
 437 from two patients from the start to the end of surgery. The white dashed line denotes the
 438 frequency of maximum of α -activity illustrating the shape of a smile. (C) Estimated effect-site
 439 concentrations of the administered anaesthetic propofol (red), sevoflurane (black), and fentanyl
 440 (blue), over the time course of surgery. In each panel, the left and right arrows mark the point of
 441 loss of consciousness and emergence from unconsciousness in the subject, respectively. Unit of
 442 fentanyl concentration is ng/ml, unit of propofol concentration is $\mu\text{g/ml}$ and unit of sevoflurane is
 443 MAC (Minimum Alveolar Concentration).

444

445 *Simulated EEG and neuronal spiking output from the frontal thalamo-cortical model*

446 Broadband neural activity has been associated with large-scale connectivity motifs (32), whereas it
447 has been suggested that increased neural fluctuation variance is the signature of a more segregated
448 brain functional connectivity. Such segregated connectivity has been linked with increased
449 correlated brain activity and spectral power (33). To represent the broadband activity in our model
450 and in order to keep our results as generic as possible, we treated this exogenous broadband input
451 in our model as random fluctuations; since the temporal and spatial correlation structure is not
452 known.

453 In order to understand the role played by these broadband fluctuations on neural activity during
454 anaesthesia, we analysed a thalamo-cortical neural model that exhibits the joint features of generic
455 cortical and subcortical networks (Eqs. (4)). The action of anaesthetic drugs (e.g. propofol or
456 sevoflurane) was modelled in two stages: fluctuation variance reduction, and synaptic inhibition.
457 Firstly the fluctuation variance of exogenous inputs to the system ('neural noise') was decreased, cf.
458 Fig. 4A (lower panel). The evolution and spectral properties of synchronous patterns were
459 recorded for each epoch. This showed an induction of β -band activity followed by a generic
460 deceleration of oscillatory activity, transitioning from the β band to the α band (Fig. 4A). An
461 increase of the fluctuation level – as would occur when the concentration of anaesthetic drugs
462 decrease – inverts the characteristic spectral features; giving rise to a spectrogram pattern like the
463 characteristic anaesthetic "smile" in Fig. 2. The second modelled effect of anaesthetic drugs was to
464 follow much previous literature and cause an increase in inhibitory synaptic gain. Figure 2B reveals
465 that additional synaptic anaesthetic action does not qualitatively change the simulated EEG.



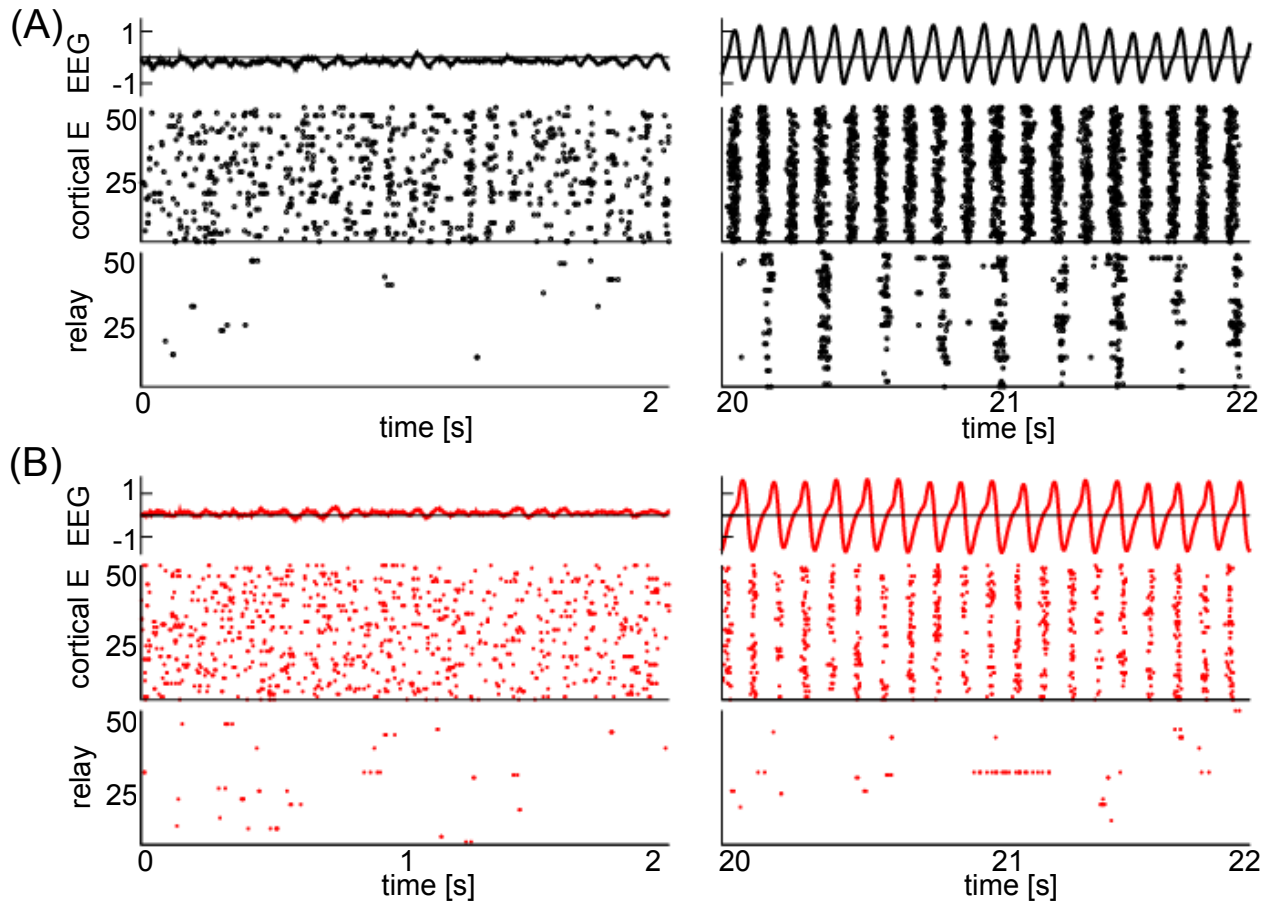
466

467 Figure 4: Numerical simulation of frontal EEG based on the frontal spiking neuron network model.
 468 (A) global drive by random fluctuations (B) global drive by random fluctuations with additional
 469 anaesthetic synaptic action. Spectral power of EEG (top panel) is given together with time-
 470 dependent fluctuation variance (bottom panel).

471

472 The latter results show that weakening fluctuations induce oscillations in the cortical dendritic
 473 activity. In parallel spikes synchronize rhythmically both the cortex and thalamus. Figure 5
 474 illustrates this finding in the spiking activity of a subset of neurons in the spiking network model in
 475 the absence of anaesthetic synaptic action (A). Initially, at high fluctuation variance (left panels),
 476 spiking is irregular and asynchronous but becomes more regular after some time when fluctuation
 477 variance decreases (right panels). At minimum fluctuation variance, the cortical E-cells burst with
 478 an inter-burst rhythm of 9Hz. The thalamic LGN cells burst at a rate of 4.5Hz, i.e. half of the burst
 479 firing rate of cortical neurons, and they synchronize with every second burst of cortical neurons.
 480 Simulated EEG weakly synchronizes with cortical E cell spiking at large fluctuation variance,
 481 whereas it strongly synchronizes with E cell spikes at low fluctuation variance. Adding anaesthetic

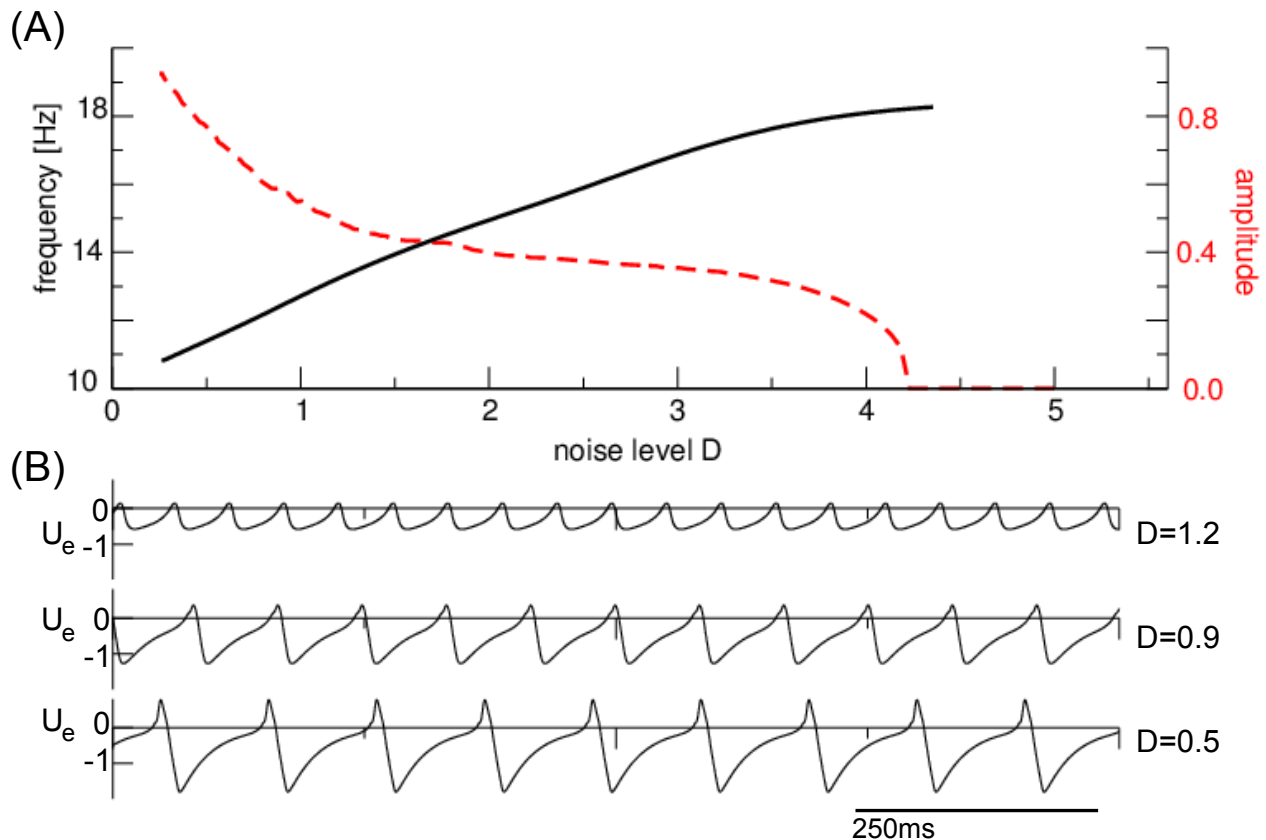
482 synaptic action (B) aligns few cortical spike trains in the E-population at low fluctuation variance.
 483 The aligned spike trains exhibit sparse burst activity; much less synchronous than under absence of
 484 anaesthetic synaptic action. LGN cells cease to spike regularly and almost stop spiking due to the
 485 increased synaptic inhibition. Similar to (A), EEG still synchronizes well with E cell spiking activity.



486
 487 Figure 5: Increasing regularity of frontal EEG and spiking activity in frontal cortex and thalamus
 488 with increasing time and decreasing amplitude of random fluctuations. (A) global drive by random
 489 fluctuations (B) global drive by random fluctuations with additional anaesthetic synaptic action.
 490 The fluctuation level decreases according to Fig. 2, bottom panel. For better visualization, panels
 491 show spike events of 50 neurons only arbitrarily chosen in each neural structure. 'E' = excitatory
 492 neurons. 'relay' = thalamo-cortical relay neurons in the LGN.

494 Encephalographic activity represents the collective activity of neurons populating superficial
 495 cortical networks. To understand better the fluctuation-induced spectral change observed in Figs. 3
 496 and 4, we performed a mean-field analysis of a reduced cortical spiking network subjected to
 497 additive noise.

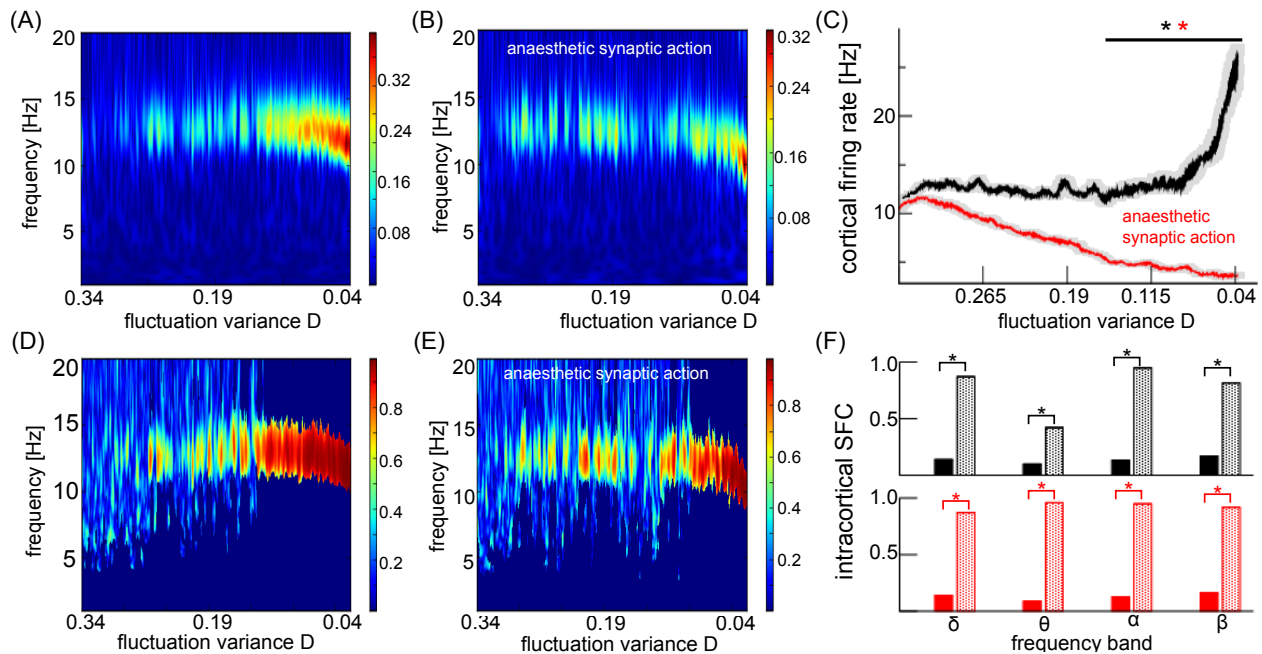
498



499
 500 Figure 6: Random fluctuation-induced smile effect originates from an underlying oscillatory
 501 instability (Hopf bifurcation). (A) The amplitude (red) and frequency (black) of deviations $U_e(t)$
 502 from the systems stationary state are computed numerically based on the mean-field model, see
 503 Eqs. (5). The large value of D compared to Fig. 4 and 5 compensates for the missing fluctuations
 504 input from the thalamus - which is included in the full spiking model. (B) Simulated mean-field EEG
 505 subjected to different noise levels.

506 We find that, at high fluctuation levels ($D > 4.2$), the system does not oscillate and deviations from
 507 the stationary state have zero amplitude, cf. Fig. 6. Decreasing the fluctuation level induces loss of
 508 stability (Hopf bifurcation) resulting in increasing amplitude, initially in the β -band, but then
 509 slowing to the α -band. A noise-induced instability has been found recently in more simple neural
 510 models (39). Hence additive fluctuations alone are able to produce a shift in the network stability
 511 which is reflected by the observed changes in the system frequency and oscillation amplitude. This
 512 explains the frequency and magnitude tuning by modified fluctuation variance in the full model
 513 observed in Figs. 3-5.

514



515

516 Figure 7: Spectral power, firing rate and synchronization in the frontal cortex with decreased
 517 fluctuation variance. (A) Power spectrum without anaesthetic synaptic action. (B) Power spectrum
 518 with anaesthetic synaptic action. (C) Mean population firing rate of E-cells. Error bars (grey) denote
 519 standard errors, firing rates below the horizontal bar are significantly different to firing rates at
 520 largest fluctuation variance ($p < 0.001$, Kruskal-Wallis test) (D) Global phase synchrony of simulated
 521 LFPs without anaesthetic synaptic action. (E) Global phase synchrony of simulated LFPs with

522 anaesthetic synaptic action. (F) Intra-area spike-field coherence between E-cells, error bars denote
523 standard errors. For all panels, the fluctuation variance D varies according to Fig.4, bottom panel.

524 *Connectivity in the frontal network model*

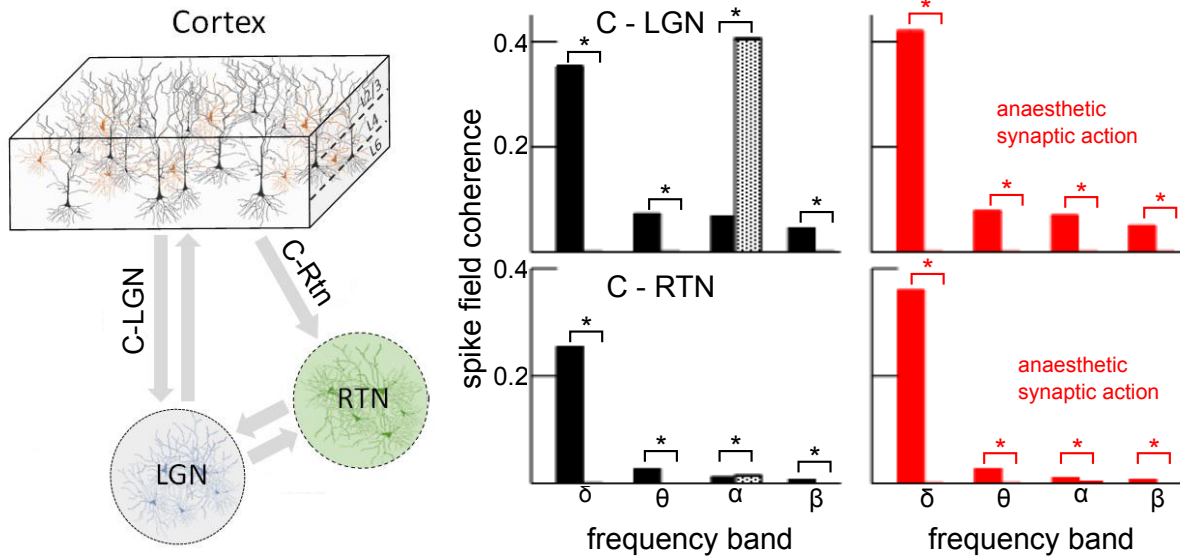
525 To better illustrate intra-cortical dynamics, Fig. 7 shows the spectral power (A) and the population
526 firing rate (C, black) of dendritic activity in the modelled cortical excitatory neuronal population
527 without synaptic anaesthetic action. The power and the firing rate ($p < 0.001$) increases as the
528 fluctuation variance decreases. The corresponding intra-area phase locking index of dendritic
529 activity (D) between excitatory cells in the cortical area reveals a monotonic phase synchronization
530 enhancement as fluctuation variance decreases. Similarly, weakening fluctuations enhances the
531 intra-area SFC (F, black) in all frequency bands dramatically. This increase of intra-area SFC
532 coincides with increasing phase synchrony (see panel D) when the peak of maximum spectral EEG
533 power (panel a) shifts from the β -band to the α -band.

534 Considering anaesthetic action on the inhibitory synaptic gain in addition, the power surge (B),
535 phase synchrony (E) in the β -and α -band and SFC (F, red) are retained; but we now see a more
536 realistic statistically significant ($p < 0.001$) decrease in the population firing rate (C, red). This
537 decrease of firing rate is in line with experimental findings in the cortex in the presence of various
538 anaesthetic agents (21).

539
540 The cross-spike-field coherence (CSFC) *between* different populations behaves differently.
541 Weakening fluctuations markedly *diminishes* the coherence between cortical excitatory cells and
542 thalamic cells as seen in Fig. 8. In the absence of inhibitory synaptic anaesthetic action, low
543 fluctuation variance makes the CSFC vanish in all frequency bands except for the α -band where it
544 increases in the α -band. The addition of inhibitory synaptic anaesthetic action to the model

545 eliminates the spike-field coherence in all frequency bands. Hence cortex and thalamus functionally
 546 decouple.

547



548

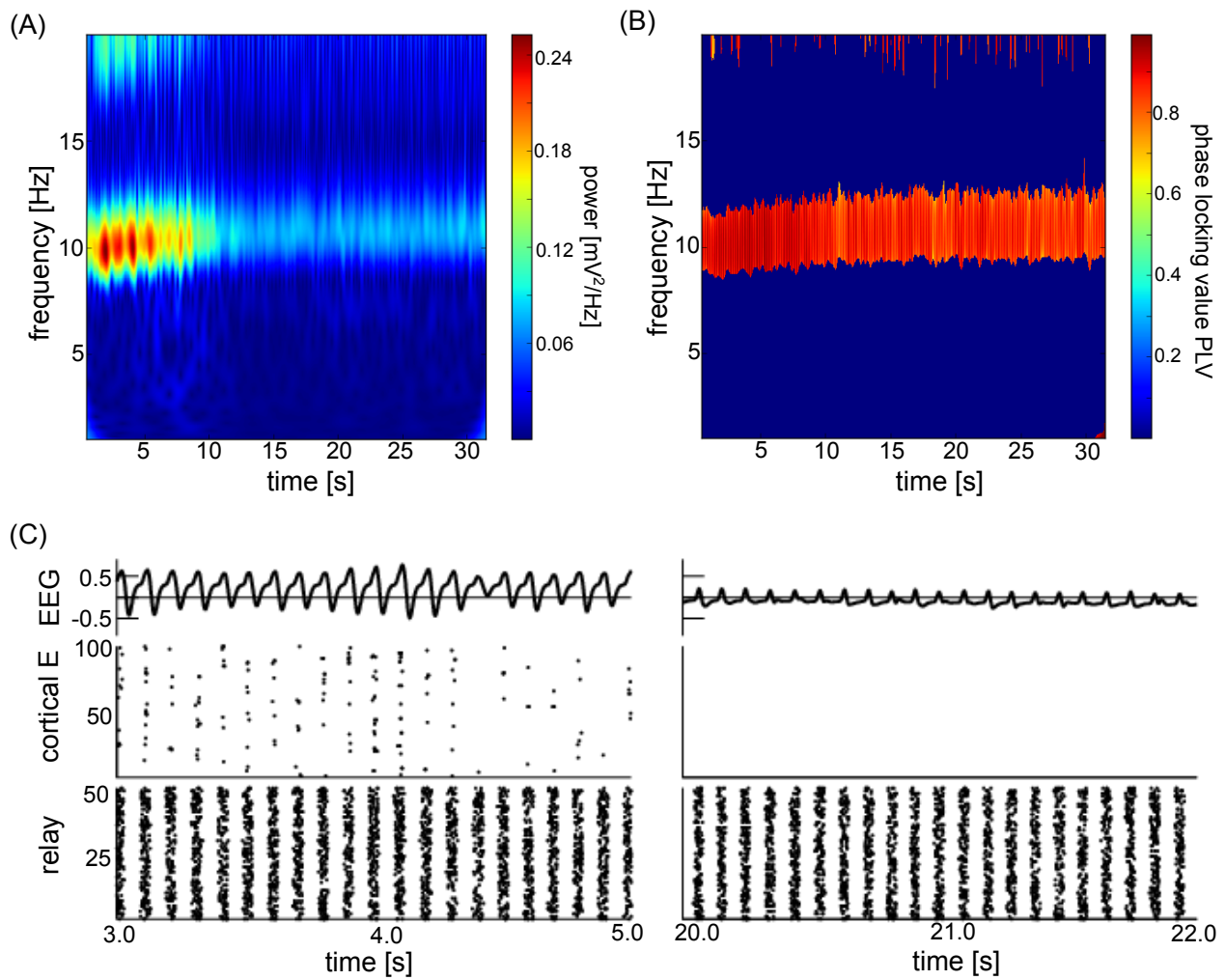
549 Figure 8: Frontal cortex and the thalamic structures decouple for weak random fluctuations. Panels
 550 on right hand side show the cross spike-field coherence between cortex and LGN (C-LGN) and
 551 between the cortex and the thalamic reticular area (C-RTN) subject to the fluctuation intensity in
 552 the absence (black) and presence (red) of anaesthetic synaptic action. Error bars denote standard
 553 errors, $p < 0.0001$ (Kruskal-Wallis test)

554

555 *Anteriorisation : EEG and intra-area connectivity in the occipital thalamo-cortical model*

556 Anaesthetics are known to not only modify frontal EEG but synchronously occipital EEG (16,35,50).
 557 Figure 9(A) shows strong activity in the α -band in the beginning (large fluctuation variance) that
 558 drops rapidly after some time (small fluctuation variance). This transition is in good accordance to
 559 experimental data (16,35). Since this posterior α -activity drops while the anterior α -activity

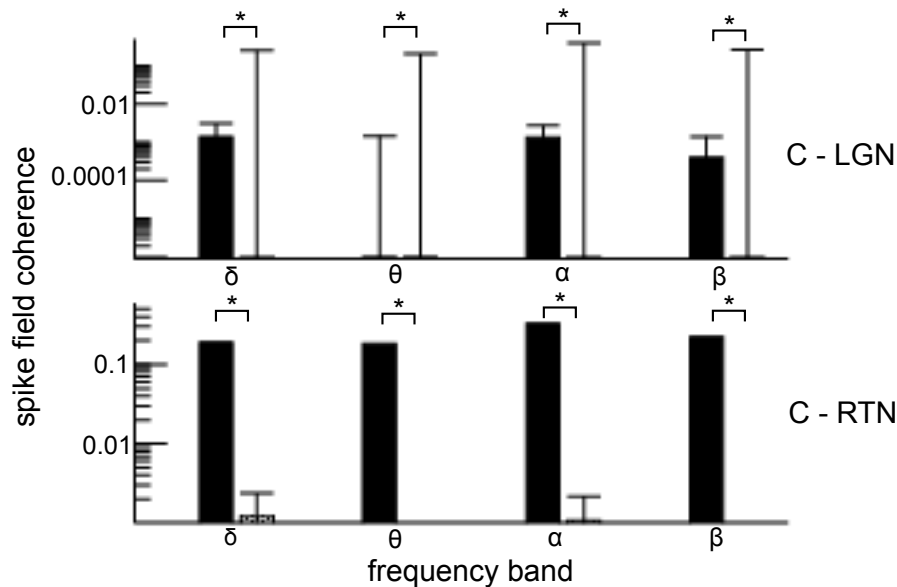
560 emerges (see previous sections), this effect is called anteriorization (50). The occipital α -rhythm
 561 emerges from a highly synchronous E-population (Fig.9(B)) that retains its phase synchrony over
 562 time, i.e. for all fluctuation variances. The high initial α -power is accompanied by synchronous
 563 spiking in the E-population (at large fluctuation variance), whereas spiking stops at large times
 564 (low fluctuation), cf. Fig. 9(C). At a first glance, this seems to contradict the persistent strong phase
 565 synchrony between the cells. However, thalamic LGN cells spike highly synchronous persistently
 566 over time at a frequency of ~ 10 Hz driving the E population. This thalamo-cortical drive ensures the
 567 strong E-cell phase synchrony.



568

569 Figure 9: Occipital α -activity drops with increasing fluctuation variance while LGN activity is
 570 retained. (A) Time-frequency distribution of numerically simulated EEG. (B) Global phase
 571 synchrony in the E population. (C) EEG time series (top panel), spiking activity in a subset of 100
 572 cortical E cells (centre panel) and in a subset of 50 LGN cells (bottom panel).

573 To understand better network interactions under anaesthesia, it is insightful to take a closer look at
 574 inter-area connectivity. Figure 10 reveals the fragmentation of occipital cortex and the thalamic
 575 areas PGN and RTN.



576
 577 Figure 10: Inter-area connectivity between occipital cortex and the thalamic areas in different
 578 frequency bands. The solid and dotted bars denote the median spike field coherence (SFC) at high
 579 ($D=1.0$) and low ($D=0.01$) fluctuation variance, vertical bars denote the standard error. All SFC
 580 distributions in all frequency bands at high and low fluctuation variances are significantly different
 581 ($p < 0.00001$).

582

583 **Discussion**

584 **Model description of experimental EEG data**

585 The model we propose here is able to reproduce a number of observed characteristics of
586 propofol/sevoflurane anaesthesia. It describes the characteristic changes in EEG power and
587 frequency in the β - and α - frequency range, the increase in local neuronal intra-population
588 synchrony combined with loss of distant neuronal inter-population synchrony, and the decrease in
589 neuronal firing rate.

590

591 Previous experimental studies on the effect of general anaesthetics have shown an initial induction
592 of enhanced neural activity in the β frequency range with a subsequent peak frequency decrease to
593 the α -frequency band – the so-called smile effect or travelling peak mechanism (34) – with
594 changing anaesthetic concentrations (13, 16, 17, 35). Examples of this phenomenon are shown in
595 Figure 3. During this transition subjects typically lose consciousness. In recent years, many studies
596 have focussed on the reverse transition from unconsciousness back to consciousness and usually
597 revealed a reversal of these spectral characteristics (15, 35).

598

599 Our results show that time-frequency characteristics in the β and α frequency range can be
600 explained by a state-dependent change in broadband neural activity. The onset of β -activity and the
601 subsequent frequency decrease into the α -range can be explained by a transition from a stable to an
602 unstable oscillatory neural state, cf. Fig. 6.

603 The intra-population phase synchrony of the model EEG increases with decreasing fluctuation
604 intensity (Fig. 6) both in the absence and presence of anaesthetic inhibitory synaptic effects. This is
605 in line with experimental findings of enhanced EEG-coherence in the α band at large dose of
606 propofol (16).

607

608 Unlike the EEG patterns – which seem to be largely driven by levels of neural fluctuations –

609 neuronal ensemble spiking activity is more sensitive to the anaesthetic enhancement of inhibitory
610 synaptic effects. When the input fluctuations weaken cortical neurons start bursting synchronously,
611 but their synchrony weakens with increased anaesthetic inhibitory synaptic action (Figs. 5 and 7).
612 This is also reflected in their population firing rate which first decreases, but subsequently
613 increases as fluctuation variance is further decreased (if no anaesthetic synaptic action is included
614 in the model). Conversely the population firing rate decreases monotonically if increasing
615 anaesthetic synaptic inhibition is added to the model. These different effects indicate that it is the
616 relative level of fluctuation variance and anaesthetic inhibitory synaptic action that determines the
617 population firing rate. This finding corroborates the results of a previous experimental study (17)
618 which showed a wide range of firing rates in the prefrontal cortex after LOC in different patients –
619 both below and beyond the firing rate measured before LOC.

620

621 Relay cells in the LGN exhibit synchronous bursts in the absence of anaesthetic synaptic action. This
622 is in line with the burst activity observed experimentally in thalamic LGN neurons of un-
623 anaesthetized animals (36) and in non-REM sleep stages (37). Such burst-like activity in the LGN
624 has been postulated to block meaningful information transfer to the cortex (38). However under
625 anaesthetic synaptic action, LGN cells reduce their firing activity dramatically (Figs. 5 and 7).

626

627 One of the strengths of our approach is that the phenomenon we describe is fundamentally driven
628 by changes in pre-synaptic firing rates while assuming a generic neuron model. Hence the results
629 are robust to variations in neuron model parameters and does not require fine tuning. The
630 population dynamics predicted by our model are diverse and comprise both irregular firing and
631 bursting, originating from circuit interaction. This can be generated and altered in many ways, and
632 thus does not depend specifically on the neuron model we have chosen; or indeed the specific
633 neuronal effects of each different anaesthetic drug.

634

635 **Link between anaesthetic action and intrinsic fluctuation variance**

636

637 Using human data, and building on the well-known experimental finding that most anaesthetics
638 affect single neurons and populations by specific receptor and ion channel action (21), our work
639 departs from previous modelling studies by introducing the notion that a *generic decrease in neural*
640 *fluctuations* in the global brain network originating in the ascending arousal system may tune the
641 transitions observed under anaesthesia. A converging line of evidence indicates that anaesthesia
642 enhances the overall inhibition in the brain stem, which triggers a reduction in random input to the
643 cortex and the thalamus (39). In the current debate on the question of whether general anaesthetics
644 act primarily at cortical or subcortical levels, our model would lend support to the importance of
645 subcortical actions. It would also suggest that a progressive frontal increase in α -frequency as
646 anaesthesia concentration decreases at the end of surgery, could be a biomarker of gradual increase
647 in AAS activity, that is associated with a good post-operative recovery (40). This is also supported
648 by our finding that decreasing AAS induces a drop of α -power in occipital areas in very good
649 accordance to experimental data (16,35). Conversely, failure to show an increase in peak frequency
650 before waking might be an indication that the subcortical structures have not activated in the
651 correct order and are unprepared for the arousal – and hence is associated with more
652 postoperative delirium.

653

654 **Intra- and inter-area functional connectivity**

655

656 Large random fluctuations in a system result in broadband neural activity, which is associated with
657 large-scale connectivity motifs involving a plurality of time scales (32). This allows brain circuits to
658 explore their dynamic repertoire (41). Figure 7 reveals strong increases in phase synchrony of

659 electric potentials in the α -band *within* the cortical population at low fluctuation variance (i.e.
660 during anaesthesia); which agrees with experimental studies demonstrating strong synchronized
661 frontal α -activity close to the point of loss of consciousness (16, 35) and increased regional
662 synchrony under sedation (52,53). The intra-area neuronal spike-field coherence quantifies
663 functional connectivity based on the synchrony between spikes and co-localized electric potentials.
664 Weak input fluctuations yield high coherence between cortical cells both with and without the
665 inclusion of anaesthetic synaptic action in the model.

666

667 Considering inter-area connectivity, the cross-spike-field coherence between cortical and thalamic
668 areas vanishes at low fluctuation variances with anaesthetic synaptic action, cf. Fig. 8, indicating a
669 functional isolation of cortex from thalamus during anaesthesia. Such a decoupling between cortical
670 and subcortical populations has been hypothesized theoretically (42) and adds to a growing body
671 of evidence in sleep (42) and in anaesthesia (17, 43). Our results thus supports that de-noising the
672 brain functionally decouples it and hence renders it more regular. This aligns with recent
673 experimental results (44): studying local field potentials in ferrets under anaesthesia, the authors
674 found reduced information transfer between prefrontal cortex and visual cortex with increased
675 anaesthetic concentration. This decrease was associated with augmented active information
676 storage (AIS) and reduced differential entropy (DE) in each area. Large AIS represents much stored
677 information while low DE reflects less available information to be transferred. In this information
678 theoretic framework, the enhanced intra-area functional connectivity observed experimentally in
679 EEG and found in our model as augmented phase synchrony represents increased AIS and hence
680 reduces the information that can be transferred. Moreover, a previous functional magnetic
681 resonance imaging study (45) found a reduced repertoire of internal brain states under propofol
682 anaesthesia. This is in line with the increased AIS and with suggested role of broadband neural
683 activity in exploring the dynamical repertoire of neural networks (41). In addition, these results are

684 in agreement with the reported fact that random fluctuations - or neural variability - is beneficial to
685 information processing and, consequently, less variability reduces the information flow between
686 neural structures (46). Taken together, our work complements these studies by showing that
687 weakening fluctuations not only hampers information flow between neural populations but
688 consequently splits up interconnected networks.

689 In sum, our results show that weak fluctuations in the brain circuit cause a nonlinear oscillatory
690 instability, yielding a local intra-area synchrony in the α frequency band. This intra-area synchrony
691 disrupts synchrony between cortex and thalamus and hence fragments the various populations
692 involved. Since the LGN is the relay structure of information flow, we conclude that its synchrony
693 loss to the cortex contributes primarily to the loss of consciousness.

694

695 **Perspectives of the model**

696

697 Other studies on the origin of sleep-wake transitions have highlighted the importance of the AAS
698 (47) controlling the brain excitation level. Various specific aminergic and cholinergic nuclei of the
699 AAS originate in the brainstem and innervate both the cortex and the thalamus, activating LGN
700 neurons as well as the reticular nuclei. Our proposed model takes into account noisy thalamic and
701 cortical input assuming that broadband neural activity in the thalamo-cortical system is controlled
702 by the brainstem; but it could equivalently be considered as coming from other uncorrelated
703 distant cortical sources. This points to a synergistic interaction between the increased GABA effects
704 of anaesthetic drugs and the decrease in neuronal fluctuations. The increased hyperpolarisation in
705 distant brain structures, caused by the GABAergic actions, *will themselves* cause decreased
706 fluctuations in the input to the region of brain under consideration. Thus the observed changes in
707 EEG pattern might be secondary to GABAergic actions at a distant region. As an aside, the model
708 proposed fits well with the known effects of ketamine on the EEG. This drug causes an increase in

709 alpha frequency and then loss of α -power, presumably the result of its known effect of increasing
710 brain stem noise input to the thalamus and cerebral cortex. However the causes of ketamine-
711 induced cortical segmentation are not explained by our model, and remain an enigma.

712

713 The proposed spiking population model and the derived mean-field model consider homogeneous
714 spatial neural populations. This homogeneity approximation is valid for describing EEG spectra
715 (33). More detailed experimental studies focussing on the spatio-temporal evolution of Local Field
716 Potentials in rats under isoflurane anaesthesia have discovered a sequence of meta-stable neural
717 states during the emergence phase (48). These meta-stable states are spatial patterns that are
718 activated in a specific temporal sequence. Since meta-stable states require specific non-
719 homogeneous network interactions (49) while the present model network is homogeneous, such
720 meta-stable states are not solutions of our model, but may be elements of future work.

721

722 Previous network studies of coupled individual neurons have also reproduced qualitatively frontal
723 and EEG (8) and anteriorisation (50) by considering anaesthetic effects in individual neurons. Even
724 neural mass network models have been shown to reproduce both frontal EEG spectral features and
725 anteriorisation (51). To our best knowledge, the present study is one of the first to involve the AAS
726 demonstrating its importance. We have considered both frontal and occipital cortical areas, but
727 have neglected other brain areas that are known to exhibit diverse anaesthetic impact. Examples
728 are the parietal cortex and the areas of the default mode network that respond differently at
729 different anaesthetic depths (52,54). Moreover the work does not consider deep anaesthesia where
730 other characteristic features emerge such as burst suppression, slow frequencies ($<1\text{Hz}$), an intra-
731 area fragmentation (52) or isoelectric activity (55).

732

733 As a conclusion, the present work proposes that anaesthetic action modifies the global regularity of

734 intrinsic neural activity. Increasing anaesthetic concentration decreases broadband fluctuations,
735 enhances the coherence of intra-area neural activity, and induces a functional decoupling of the
736 thalamo-cortical circuit. The parallel increase in intra-area functional connectivity accompanied by
737 a reduction of functional connectivity between network areas is a direct consequence of amplified
738 correlations in neural activity.

739

740 **Acknowledgements**

741 This work has been supported by the Natural Sciences and Engineering Research Council of Canada
742 (JL).

743

744 **Contributions**

745 All authors designed the study, analysed the data, and wrote the paper.
746

747 **Competing interests**

748 We state that there are no competing interests.

749 **Declaration of interests:**

750 None.

751

752

753 **References**

- 754 1. Grasshoff C, Drexler B, Rudolph U and Antkowiak B (2006). Anaesthetic drugs: linking molecular
755 actions to clinical effects. *Curr. Pharm. Des.* 12(28) : 3665-3679
- 756 2. Alkire MT, Hudetz AG and Tononi G (2008). Consciousness and Anesthesia. *Science* 322 : 876 -
757 880. doi :10.1126/science.1149213
- 758 3. Sellers K, Bennett D, Hutt A, Williams J and Frohlich J (2015). Awake versus Anesthetized: Layer-
759 Specific Sensory Processing in Visual Cortex and Functional Connectivity between Cortical Areas, *J.*
760 *Neurophysiol.* 113(10): 3798-815.
- 761 4. Barttfeld P, Uhrig L, Sitt JD, Sigman M, Jarraya B and Dehaene S (2015) Signature of
762 consciousness in the dynamics of resting-state brain activity, *Proc. Natl. Aca. Sci. USA* 112(3) : 887-
763 889. Doi : 10.1073/pnas.1418031112
- 764 5. Schultz A, Siedenberg M, Grouven U, Kneif T and Schultz B (2008). Comparison of Narcotrend
765 Index, Bispectral Index, spectral and entropy parameters during induction of propofol-remifentaniol
766 anaesthesia, *J. Clin. Monit. Comput.* 22 :103-111.
- 767 6. Hight D, Voss LJ, Garcia PS and Sleight J (2017). Changes in Alpha Frequency and Power of the
768 Electroencephalogram during Volatile-Based General Anesthesia. *Front. Syst. Neurosci.* 11 :36. doi :
769 10.3389/fnsys.2017.00036
- 770 7. McCarthy MM, Brown EN and Kopell N (2008). Potential Network Mechanisms Mediating
771 Electroencephalographic Beta Rhythm Changes during Propofol-Induced Paradoxical Excitation. *J.*
772 *Neurosci.* 28(50) : 13488-13504.
- 773 8. Ching S, Cimenser A, Purdon PL, Brown EN and Kopell NJ (2010). Thalamocortical model for a
774 propofol-induced-rhythm associated with loss of consciousness. *Proc. Natl. Acad. Sci. USA* 107(52):
775 22665-22670.

- 776 9. Bojak I, Day HC and Liley DTJ (2013). Ketamine, propofol, and the EEG: a neural field analysis of
777 HCN1-mediated interactions. *Front. Comput. Neurosci.* 7: 22
- 778 10. Hashemi M, Hutt A and Sleigh S (2014). Anesthetic action on extra-synaptic receptors: effects in
779 neural population models of EEG activity. *Front. Syst. Neurosci.* 8, 232. doi:
780 10.3389/fnsys.2014.00232
- 781 11. Hendrickx JF, Eger EI, Sonner JM and Shafer SL (2008). Is synergy the rule? A review of
782 anesthetic interactions producing hypnosis and immobility. *Anesth. Analg.* 107(2) :494-506 . doi:
783 10.1213/ane.0b013e31817b859e
- 784 12. Steriade M, Amzica F, Contreras D (1994). Cortical and thalamic cellular correlates of
785 electroencephalographic burst-suppression. *Electroencephalogr. Clin. Neurophysiol.* 90:1-16.
- 786 13. Sellers KK, Bennett DV, Hutt A and Fröhlich F (2013). Anesthesia differentially modulates
787 spontaneous network dynamics by cortical area and layer. *J. Neurophysiol* 110:2739-2751.
788 doi:10.1152/jn.00404.2013
- 789 14. Hudetz AG, Liu X, Pillay S, Boly M, Tononi G (2016). Propofol anesthesia reduces Lempel-Ziv
790 complexity of spontaneous brain activity in rats. *Neurosci Lett.* 628:132-5. doi:
791 10.1016/j.neulet.2016.06.017
- 792 15. Vizuete JA, Pillay S, Ropella KM and Hudetz AH (2014). Graded Defragmentation of cortical
793 neuronal firing during recovery of consciousness in rats. *Neuroscience* 275 : 340-351. doi :
794 10.1016/j.neuroscience.2014.06.018
- 795 16. Cimenser A, Purdon PL, Pierce ET, Walsh JL, Salazar-Gomez AF, Harrell PG, Tavares-Stoeckel C,
796 Habeeb K and Brown EM (2011) Tracking brain states under general anesthesia by using global
797 coherence analysis , *Proc. Natl. Aca. Sci. USA* 108(21) : 8832–8837. doi: 10.1073/pnas.1017041108

- 798 17. Lewis LD, Weiner VS, Mukamel EA, Donoghue JA, Eskandar EN, Madsen JR, Anderson WS
799 Hochberg LR, Cash SS, Brown EN and Purdon PL (2012) Rapid fragmentation of neuronal networks
800 at the onset of propofol-induced unconsciousness. *Proc. Natl. Acad. Sci. USA*109(49):19891–19892.
801 doi: 10.1073/pnas.1210907109
- 802 18. Alkire MT and Miller J (2005). General anesthesia and the neural correlates of consciousness.
803 *Prog Brain Res.* 150:229-44.
- 804 19. Brown EN, Lydic R and Schiff ND (2010) General Anesthesia, Sleep and Coma. *N. Engl. J. Med.*
805 363: 2638-2650.
- 806 20. Saper CB, Scammell TE, Lu J. (2005) Hypo-thalamic regulation of sleep and circadian rhythms.
807 *Nature* 437:1257-63
- 808 21. Franks NP (2008) General anaesthesia: from molecular targets to neuronal pathways of sleep
809 and arousal. *Nat Rev Neurosci.* 9(5):370-86. doi: 10.1038/nrn2372.
- 810 22. Kopanitsa MV (1997). Extrasynaptic receptors of neurotransmitters: distribution, mechanisms
811 of activation, and physiological role. *Neurophysiol.* 29 : 448–458.
- 812 23. Mitchell SJ and Silver RA (2003) Shunting inhibition modulates neuronal gain during synaptic
813 excitation. *Neuron* 38 : 433-445.
- 814 24. Hutt A and Buhry L (2014) Study of GABAergic extra-synaptic tonic inhibition in single neurons
815 and neural populations by traversing neural scales: application to propofol-induced anaesthesia. *J.*
816 *Comput. Neurosci.* 37(3) : 417-437 .
- 817 25. Amari S (1977) Dynamics of Pattern Formation in Lateral-Inhibition Type Neural Fields. *Biol.*
818 *Cybern.* 27 : 77-87
- 819 26. Lefebvre J, Hutt A, Knebel JF, Whittingstall K and Murray M (2015). Stimulus Statistics shape
820 oscillations in nonlinear recurrent neural networks. *J. Neurosci.* 35(7): 2895-2903
- 821 27. Herrmann C, Murray MM, Ionta S, Hutt A and Lefebvre J (2016) Shaping neural oscillations with

822 periodic stimulation. *J. Neurosci.* 36(9): 5328-37_

823 28. Wang XJ and Buzsaki G (1996). Gamma oscillation by synaptic inhibition in a hippocampal
824 interneuronal network model. *J. Neurosci.* 16(20) : 6402–6413

825 29. Fries P, Reynolds JH, Rorie AE, Desimone R (2001). Modulation of oscillatory neuronal
826 synchronization by selective visual attention. *Science* 291(5508):1560-3.

827 30. Lachaux JP, Rodriguez E, Martinerie J and Varela FJ (1999). Measuring phase synchrony in brain
828 signals. *Human Brain Map.* 8: 194-208

829 31. Hutt A and Munk MHJ (2007). Mutual phase synchronization in single trial data. *Chaos and*
830 *Complexity Letters* 2 (2/3): 225-246.

831 32. Voytek B, Kayser AS, Badre D, Fegen D, Chang EF, Crone NE, Parvizi J, Knight RT and D’Esposito
832 M (2015). Oscillatory dynamics coordinating human frontal networks in support of goal
833 maintenance. *Nature Neurosci.* 18:1318-1324. doi: 10.1038/nn.4071

834 33. Deco G, Jirsa VK, Robinson PA, Breakspear M and Friston K. (2008). The dynamic brain: from
835 spiking neurons to neural masses and cortical fields. *PLoS Comput Biol.* 4(8):e1000092. doi:
836 10.1371/journal.pcbi.1000092

837 34. Scheib MC (2017) Brainstem influence on thalamocortical oscillations during anesthesia
838 emergence. *Front. Syst. Neurosci.* 11 :66 .

839 35. Purdon PL, Pierce ET, Mukamel EA, Prerau MJ, Walsh JL, Wong KFK, Salazar-Gomez AF, Harrell
840 PG, Sampson AL, Cimenser A, Ching S, Kopell NJ, Tavares-Stoeckel C, Habeeb K, Merhar R and
841 Brown EN (2012). Electroencephalogram signatures of loss and recovery of consciousness from
842 propofol. *Proc. Natl. Acad. Sci. USA* 110(12): E1142–E1151

843 36. Sherman SM (2001). Tonic and burst firing: dual modes of thalamocortical relay. *Trends*

844 *Neurosci.* 24:122–126.

845 37. McCormick DA and Bal T (1997). Sleep and arousal : thalamocortical mechanisms. *Annu. Rev.*
846 *Neurosci.* 20: 185–215.

847 38. Livingstone MS and Hubel DH (1981). Effects of sleep and arousal on the processing of visual
848 information in the cat. *Nature* 291:554–561.

849 39. Zecharia AY and Franks NP (2009). General anesthesia and ascending arousal pathways.
850 *Anesthesiology* 111(4):695-6. doi: 10.1097/aln.0b013e3181b061bc.

851 40. Chander D, Garcia PS, MacColl JN, Illing S and Sleight JW (2014). Electroencephalographic
852 variation during end maintenance and emergence from surgical anesthesia. *PLoS One.*
853 9(9):e106291. doi: 10.1371/journal.pone.0106291.

854 41. Ghosh A, Rho Y, McIntosh AR, Kötter R and Jirsa VK (2008). Noise during Rest Enables the
855 Exploration of the Brain Dynamic Repertoire. *PLoS Comput. Biol.* 4(10): e1000196. Doi :
856 10.1371/journal.pcbi.1000196

857 42. Tononi G, Boly M, Massimini M and Koch C (2014) Integrated information theory : from
858 consciousness to its physical substrate. *Nature Rev. Neurosci.* 17 (7): 450–461.
859 doi:10.1038/nrn.2016.44

860 43. Massimini M, Ferrarelli F, Huber R, Esser SK, Singh H and Tononi G (2005) Breakdown of
861 Cortical Effective Connectivity During Sleep. *Science* 309 :2228.

862 44. Wollstadt P, Sellers KK, Rudelt L, Priesemann V, Hutt A, Frohlich F and Wibral MI
863 (2017). Breakdown of local information processing may underlie isoflurane anesthesia effects.
864 *PLoS Comp. Biol.* 13(6): e1005511. doi :10.1371/journal.pcbi.1005511

865 45. Hudetz AG, Liu X, Pillay S (2015) Dynamic repertoire of intrinsic brain states is reduced in

866 propofol-induced unconsciousness. *Brain Connect.* 5(1):10-22. doi: 10.1089/brain.2014.0230

867 46. Stein RB, Gossen ER and Jones KE (2005). Neuronal variability : noise or part of the signal ?
868 *Nature Rev. Neurosci.* 6 :389-397. doi : 10.1038/nrn1668

869 47. Fuller P, Sherman D, Pedersen NP, Saper CB and Lu J (2011) Reassessment of the structural
870 basis of the ascending arousal system. *J. Comp. Neurol.* 519(5): 933-956

871 48. Hudson AE, Calderon DP, Pfaff DW and Proekt A (2014). Recovery of consciousness is mediated
872 by a network of discrete metastable activity states. *Proc. Natl. Acad. Sci. USA* 111(25): 9283–9288.
873 doi: 10.1073/pnas.1408296111

874 49. Schwappach C, Hutt A and beim Graben P (2015). Metastable dynamics in heterogeneous neural
875 fields. *Front. Syst. Neurosci.* 9:97. doi: 10.3389/fnsys.2015.00097

876 50. Vijayan S, Ching S, Purdon PL, Brown EN and Kopell NJ (2013). Thalamocortical Mechanisms for
877 the Anteriorization of Alpha Rhythms during Propofol-Induced Unconsciousness. *J. Neurosci.*
878 33(27):11070 –11075

879 51. Hashemi M, Hutt A and Sleigh J (2015). How the cortico-thalamic feedback affects the EEG
880 power spectrum over frontal and occipital regions during propofol-induced anaesthetic sedation. *J.*
881 *Comput. Neurosci.* 39(1): 155

882 52. Huang Z, Liu X, Mashour GA and Hudetz AG (2018) Timescales of Intrinsic BOLD Signal
883 Dynamics and Functional Connectivity in Pharmacologic and Neuropathologic States of
884 Unconsciousness. *J. neurosci.* 38(9) :2304-2317.

885 53. Li D, Voss LJ, Sleigh JW and Li X. (2013) Effects of volatile anesthetic agents on cerebral cortical
886 synchronization in sheep. *Anesth.* 119(1):81-8.

887 54 . Liu X, Pillay S, Li R, Vizuete JA, Pechman KR, Schmainda KM and Hudetz AG (2013) Multiphasic
888 modification of intrinsic functional connectivity of the rat brain during increasing levels of propofol.

889 *Neuroimage* 83 :581-92

890 55. Altweg-Boussac T, Schramm AE, Ballestero J, Grosselin F, Chavez M, Leca S, Baulac M, Naccache
891 N, Demeret S, Navarro V, Mahon S, Charpier S (2017). Cortical neurons and networks are dormant
892 but fully responsive during isoelectric brain state. *Brain* 140:2381-2398.

893 56. Fuller PM, Sherman D, Pedersen NP, Saper CB and Lu J (2011) Reassessment of the Structural
894 Basis of the Ascending Arousal System. *J. Comp. Neurol.* 519:933–956.

895